

Estimate of emissions on road networks via Generic Second Order Models

Caterina Balzotti*

Maya Briani[§]

Benedetto Piccoli[‡]

Abstract

In this paper we provide emission estimates due to vehicular traffic via Generic Second Order Models. We generalize them to model road networks with merge and diverge junctions. The procedure consists on solving the Riemann Problem at junction assuming the maximization of the flow and a priority rule for the incoming roads. We provide some numerical results for a single-lane roundabout and we propose an application of the given procedure to estimate the production of nitrogen oxides (NO_x) emission rates. In particular, we show that the presence of a traffic lights produces a 28% increase in the NO_x emissions with respect to the roundabout.

Keywords. Second order traffic models; road networks; Riemann problem; emissions.

Mathematics Subject Classification. 35L65, 90B20, 62P12.

1 Introduction

Estimating traffic emissions is an important and challenging problem. First, emission models are based on the knowledge of acceleration of vehicles, beside speed, thus, at macroscopic level, requiring the use of the so-called second-order models. The latter consist of a first equation for conservation of mass and a second for the speed or momentum. The first second-order models go back to Payne and Whitham [22, 25], but a new of research originated starting with the Aw-Rascle-Zhang (ARZ) model [3, 26]. The latter successfully addressed criticisms of the Payne-Whitham approach [7]. More recently, various models were proposed ranging from generalizations of the ARZ such as in [12, 19, 9] to phase transition models as proposed in [5, 6] and Generic Second Order Models [19, 1]. Such models are characterized by a family of fundamental diagrams (density-flow graphs) and, due to their multi-faceted nature, they are particularly appropriate to fit real traffic data. We refer to [23, 10] for more details on data-fitted second order models.

The aim of this paper is to extend the Generic Second Order Models (GSOM) to road networks and use it for emission estimates. Traffic models on road networks have been widely studied in recent years and authors have considered many different traffic scenarios proposing a rich amount of alternative junction models. The first order Lighthill-Whitham-Richards (LWR) model [20, 24] has been extended to road networks in several papers, see for example [15, 14, 18, 8]. In [13, 16, 17] the authors analyze the second order ARZ model on networks.

In this paper we consider a road network with merge (two incoming and one outgoing roads) and diverge (one incoming and two outgoing roads) junctions. On each road the traffic flow is described by a GSOM

$$\begin{cases} \partial_t \rho + \partial_x(\rho v) = 0 \\ \partial_t w + v \partial_x w = 0, \end{cases}$$

*Dipartimento di Scienze di Base e Applicate per l'Ingegneria, Sapienza Università di Roma, Rome, Italy (caterina.balzotti@sbai.uniroma1.it).

[§]Istituto per le Applicazioni del Calcolo "M. Picone", Consiglio Nazionale delle Ricerche, Rome, Italy (m.briani@iac.cnr.it).

[‡]Department of Mathematical Sciences, Rutgers University, Camden, USA (piccoli@camden.rutgers.edu).

where $v = V(\rho, w)$ is the velocity function, ρ is the density of vehicles and w is a property of drivers. We also denote $y = \rho w$ the conserved variable called *total property*. To define the solution on the whole network we follow the approach proposed in [14] based on the concept of the Riemann Problem at a junction, which is a Cauchy problem with constant initial data on each road connected at the junction. The idea is to solve a left-half Riemann problem (waves have non-positive speed) for incoming roads and a right-half Riemann problem (waves have non-negative speed) for outgoing roads, defining the region of admissible states such that waves do not enter the junction. The identification of the solution is done by assuming the maximization of the flux and the conservation of ρ and y through the junction. The obtained maximization problem needs additional conditions depending on the considered road network to identify a unique solution. In the case of a diverge junction the unique solution is attained by fixing a distribution parameter of the flux of vehicles among the two outgoing roads. The treatment we propose in this case is similar to the one proposed in [17] for the ARZ model.

For the merge junction we propose a different approach based on a priority rule for the incoming roads. We introduce the following relation between the two incoming fluxes at the junction (q_1^+ and q_2^+), i.e.

$$q_2^+ = \frac{\beta}{1 - \beta} q_1^+,$$

for a given parameter $\beta \in [0, 1]$. The priority rule establishes which one of the two incoming roads at junction sends more flow of vehicles with respect to the other road. This assumption, coupled with the conservation of ρ and y influences the w variable. In fact, the drivers behavior of the outgoing road w_3^- is given by a convex combination of properties w_1^+ and w_2^+ of the two incoming roads, i.e.

$$w_3^- = (1 - \beta)w_1^+ + \beta w_2^+.$$

Therefore the maximal flux that can be received by the outgoing road depends on the priority rule. We proposed a new logic to obtain a solution as follows: the flow is maximized respecting the priority rule, but the latter can be relaxed if the outgoing road supply exceeds the demand of the road with higher priority. This gives rise to new solutions which can describe different traffic scenarios. For instance, when priority is ruled by the presence of traffic lights the procedure strictly respects the priority, while it allows the choice of the optimal parameter β in terms of flow maximization when priority is not strictly required as in roundabouts. The complete procedure to build the solution for a merge junction is explained in details in Definition 4.1.

To numerically test the proposed method, we use the Collapsed Generalized Aw-Rascle-Zhang (CGARZ) model [11], which fits in the framework of GSOM. Following [4] we specify as fundamental diagram a convex combination of the Newell-Daganzo or triangular fundamental diagram with the Greenshield quadratic one. We then analyze the case of a merge and diverge junction and we combine them to build a simple roundabout. Finally we propose an application of the traffic theory to estimate the nitrogen oxides (NO_x) emissions due to vehicular traffic. The interest on NO_x gases is due to their negative effects on health [27] and to their connection to ozone [2]. Here we extend the results obtained in [4] to a road network. In particular, we analyze the impact produced by the presence of traffic lights on the incoming roads into the roundabout, comparing the emission rates produced with and without them. The numerical tests show the great impact that traffic lights have on NO_x emission rates, resulting in a 28% increase compared to emissions without traffic lights. This procedure can be applied to any other pollutant associated to vehicle traffic.

The paper is organized as follows. In Section 2 we introduce the GSOM and in Section 3 the Riemann problem at junction. In Section 4 we define the solution to the Riemann problem for junctions with one incoming road and one outgoing road, one incoming road and two outgoing roads and two incoming roads and one outgoing road. In Section 5 we show some numerical tests and in Section 6 we apply the proposed model to estimate NO_x emissions.

2 Traffic model

In this work we extend the Generic Second Order Models (GSOM) [19] to road networks. We denote by GSOM a family of macroscopic traffic models which are described by a first order Lighthill-Whitham-Richards (LWR) model [20, 24] with variable fundamental diagrams. Such models are defined by

$$\begin{cases} \partial_t \rho + \partial_x(\rho v) = 0 \\ \partial_t w + v \partial_x w = 0 \end{cases} \quad (2.1)$$

with $v = V(\rho, w)$,

where $\rho(x, t)$, $v(x, t)$ and $w(x, t)$ represent the density, the speed and a property of vehicles advected by the flow, respectively, and V is a specific velocity function. The first equation of (2.1) is the conservation of vehicles, the second one is the advection of the attribute of drivers, which defines their driving aptitude by means of different fundamental diagrams. Indeed, the variable w identifies the flux curve $Q(\rho, w)$ and thus the speed of vehicles $V(\rho, w) = Q(\rho, w)/\rho$ which characterizes the behavior of drivers. System (2.1) is written in conservative form as

$$\begin{cases} \partial_t \rho + \partial_x(\rho v) = 0 \\ \partial_t y + \partial_x(yv) = 0 \end{cases} \quad (2.2)$$

with $v = V\left(\rho, \frac{y}{\rho}\right)$,

where $y = \rho w$ denotes the total property of vehicles.

The flux function $Q(\rho, w)$ and the velocity function $V(\rho, w) = Q(\rho, w)/\rho$ are assumed to satisfy the following properties.

- (H1) $Q(\rho, w)$ is strictly concave with respect to ρ , i.e. $\frac{\partial^2 Q}{\partial \rho^2} < 0$.
- (H2) $Q(0, w) = 0$ and $Q(\rho^{\max}, w) = 0$ for each $w \in [w_L, w_R]$, where ρ^{\max} is the maximum density of vehicles and $[w_L, w_R]$ is the domain of w , for suitable w_L and w_R .
- (H3) $Q(\rho, w)$ is non-decreasing with respect to w , i.e. $\frac{\partial Q}{\partial w} \geq 0$.
- (H4) $V(\rho, w) \geq 0$ for each w .
- (H5) $V(\rho, w)$ is strictly decreasing with respect to ρ , i.e. $\frac{\partial V}{\partial \rho} < 0$ for each w .
- (H6) $V(\rho, w)$ is non-decreasing with respect to w , i.e. $\frac{\partial V}{\partial w} \geq 0$.

Note that property (H5) is a consequence of the concavity (H1) and that (H6) is a consequence of (H3). Properties (H1) and (H2) imply that the flux curve $Q(\cdot, w)$ has a unique point of maximum for any w . We denote by $\sigma(w)$ the critical density, i.e. the density value where the flux attains its maximum $Q^{\max}(w)$. Moreover, for any ρ there exists a unique $\tilde{\rho}(w)$ such that $Q(\rho, w) = Q(\tilde{\rho}(w), w)$.

We recall now the main definitions concerning traffic models on road networks and we refer to [8, 14, 15, 18] for further details. Let us consider a junction J with n incoming and m outgoing roads $I_r = [a_r, b_r] \subset \mathbb{R}$, $r = 1, \dots, n + m$, possibly with $a_r = -\infty$ and $b_r = +\infty$. We define a network as a couple $(\mathcal{I}, \mathcal{J})$ where \mathcal{I} is a finite collection of roads I_r , and \mathcal{J} is a finite collection of junctions J .

On each road I_r , $r = 1, \dots, n + m$, the traffic dynamic is described by a GSOM (2.2) as

$$\begin{cases} \partial_t \rho_r + \partial_x(\rho_r v_r) = 0 \\ \partial_t y_r + \partial_x(y_r v_r) = 0 \end{cases} \quad (2.3)$$

with $v_r = V\left(\rho_r, \frac{y_r}{\rho_r}\right)$,

for $x \in I_r$ and $t \geq 0$. Following [17, 18], we consider a set of smooth test functions $\phi_r : I_r \times [0, +\infty) \rightarrow \mathbb{R}^2$ with compact support in $I_r = [a_r, b_r]$ which are smooth also across each junction J , i.e.

$$\phi_i(b_i) = \phi_j(a_j) \quad \text{and} \quad \partial_x \phi_i(b_i) = \partial_x \phi_j(a_j) \quad (2.4)$$

for $i = 1, \dots, n$ and $j = n + 1, \dots, m$. We define a *weak solution* of (2.3) as a couple of functions $(\rho_r(x, t), y_r(x, t))$ which satisfy

$$\begin{aligned} \sum_{r=1}^{n+m} \left(\int_0^\infty \int_{a_r}^{b_r} (\rho_r(x, t) \partial_t \phi_r(x, t) + (\rho_r(x, t) v_r(x, t)) \partial_x \phi_r(x, t)) dx dt + \int_{a_r}^{b_r} \rho_r(x, 0) \phi_r(x, 0) dx \right) &= 0 \\ \sum_{r=1}^{n+m} \left(\int_0^\infty \int_{a_r}^{b_r} (y_r(x, t) \partial_t \phi_r(x, t) + (y_r(x, t) v_r(x, t)) \partial_x y_r(x, t)) dx dt + \int_{a_r}^{b_r} y_r(x, 0) \phi_r(x, 0) dx \right) &= 0 \end{aligned} \quad (2.5)$$

for all the test functions ϕ_r satisfying (2.4), where $(\rho_r(x, 0), y_r(x, 0))$ is the initial data.

The construction of weak solutions in the sense of (2.5) is explained in detail in the following sections and it depends on the type of junction: we solve the Riemann problem for (2.3) on each road r with the following initial data

$$(\rho_r(x, 0), y_r(x, 0)) = \begin{cases} (\rho^-, y^-) & \text{for } x < x_0 \\ (\rho^+, y^+) & \text{for } x > x_0, \end{cases} \quad (2.6)$$

where only one between the left and right state is known. Depending on I_r if it is an incoming or an outgoing road, we have the following possibilities:

- If I_r is an incoming road at junction then $x_0 = b_r$ and only the left state (ρ^-, y^-) is known. In this case we look for weak solutions of (2.3) such that the waves have non-positive speed.
- If I_r is an outgoing road at junction then $x_0 = a_r$ and only the right state (ρ^+, y^+) is known. In this case we look for weak solutions of (2.3) such that the waves have non-negative speed.

The construction of a unique solution is performed by means of the maximization of the flux, as it will be clearer in the following sections.

3 Preliminaries for the Riemann problem at junction

As a first step, we study the properties of the traffic model (2.2). For convenience, we introduce the variable

$$u = u(\rho, y) = V\left(\rho, \frac{y}{\rho}\right), \quad (3.1)$$

and we rewrite the system as

$$\begin{cases} \partial_t \rho + \partial_x(\rho u) = 0 \\ \partial_t y + \partial_x(y u) = 0, \end{cases} \quad (3.2)$$

whose Jacobian is

$$DF(\rho, y) = \begin{pmatrix} u + \rho u_\rho & \rho u_y \\ y u_\rho & u + y u_y \end{pmatrix}. \quad (3.3)$$

Since it is easier to work with the couple (ρ, w) , hereafter we will use these variables. The eigenvalues of (3.3), as a function of (ρ, w) , are

$$\lambda_1(\rho, w) = V(\rho, w) + \rho V_\rho(\rho, w) \quad (3.4)$$

$$\lambda_2(\rho, w) = V(\rho, w). \quad (3.5)$$

By property (H5) follows $\lambda_1 \leq \lambda_2$ and $\lambda_1 = \lambda_2$ if and only if $\rho = 0$, thus the system is strictly hyperbolic except for $\rho = 0$.

The eigenvectors associated to the eigenvalues are

$$\gamma_1(\rho, w) = (\rho, \rho w) \quad (3.6)$$

$$\gamma_2(\rho, w) = \left(-\frac{1}{\rho} V_w(\rho, w), V_\rho(\rho, w) - \frac{1}{\rho^2} V_w(\rho, w) \right). \quad (3.7)$$

The first eigenvalue is genuinely nonlinear, i.e. $\nabla \lambda_1 \cdot \gamma_1 \neq 0$, while the second one is linearly degenerate, i.e. $\nabla \lambda_2 \cdot \gamma_2 = 0$. Hence, the curve of the first family are 1-shocks or 1-rarefaction waves, while the curve of the second family are 2-contact discontinuities.

Finally the Riemann invariants are

$$z_1(\rho, w) = w \quad (3.8)$$

$$z_2(\rho, w) = V(\rho, w). \quad (3.9)$$

The 1-shock and 1-rarefaction waves are defined by the first Riemann invariant z_1 and the 2-contact discontinuities by the second Riemann invariant z_2 .

Remark 3.1. All the Figures shown hereafter refer to a particular GSOM, the Collapsed Generalized Aw-Raschle-Zhang (CGARZ) model with the family of flux functions defined in Section 5.

In order to construct waves with non-negative or non-positive speed at junction, we study the sign of the eigenvalues defined in (3.4) and (3.5). The first eigenvalue $\lambda_1(\rho, w) = \rho + \rho V_\rho(\rho, w) = Q_\rho(\rho, w)$ is such that $\lambda_1 \geq 0$ for $\rho \leq \sigma(w)$ and $\lambda_1 < 0$ for $\rho > \sigma(w)$, by properties (H1) and (H2) of the flux function. Hence, for each $w \in [w_L, w_R]$ the 1-shocks and 1-rarefaction waves have non-negative speed for $\rho \leq \sigma(w)$ and negative speed for $\rho > \sigma(w)$. In Figure 1 we show an example of the positive and negative regions of λ_1 obtained with the flux and velocity functions defined in Section 5. The second eigenvalue $\lambda_2(\rho, w) = V(\rho, w) \geq 0$ by definition of V , thus the speed of the 2-contact discontinuities is always non-negative.

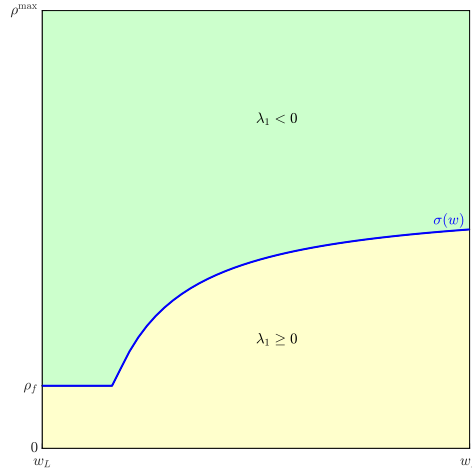


Figure 1. Example of positive (yellow-down) and negative (green-up) regions for λ_1 depending on w .

In order to maximize the flux in the following sections we will make use of the *supply* and *demand* functions. For each $w \in [w_L, w_R]$, the supply function $s(\rho, w)$ is defined as

$$s(\rho, w) = \begin{cases} Q^{\max}(w) & \text{if } \rho \leq \sigma(w) \\ Q(\rho, w) & \text{if } \rho > \sigma(w). \end{cases} \quad (3.10)$$

Analogously, we define the demand function $d(\rho, w)$ as

$$d(\rho, w) = \begin{cases} Q(\rho, w) & \text{if } \rho \leq \sigma(w) \\ Q^{\max}(w) & \text{if } \rho > \sigma(w). \end{cases} \quad (3.11)$$

In Figure 2 we show an example of the supply function on the left and of the demand function on the right.

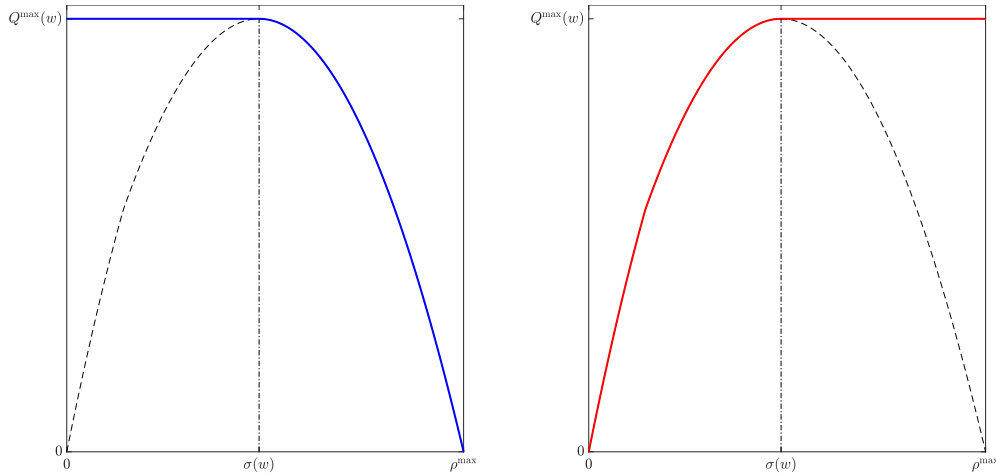


Figure 2. Supply function (left) and demand function (right).

3.1 Incoming road at the junction

Let us consider an incoming road at the junction. We are then interested only in the waves with non-positive speed. Since $\lambda_2 \geq 0$, we can just have 1-shock or 1-rarefaction waves. Let us fix a left state $U^- = (\rho^-, w^-)$, our aim is to define the set of all possible right states $U^+ = (\rho^+, w^+)$ that can be connected to U^- with a wave with non-positive speed. We denote by $\mathcal{N}(U^-)$ the set of admissible densities.

Proposition 3.1. Let $U^- = (\rho^-, w^-)$ be a left state on an incoming road. The set of possible right states $U^+ = (\rho^+, w^+)$ that can be connected to the left state lies on the level curve $\{z_1 = w^-\}$, i.e. $w^+ = w^-$, and they are such that:

1. If $\rho^- \leq \sigma(w^-)$, then ρ^+ must be in $\mathcal{N}(U^-) = [\tilde{\rho}^-(w^-), \rho^{\max}]$, where $\tilde{\rho}^-(w^-)$ is the density such that $Q(\tilde{\rho}^-(w^-), w^-) = Q(\rho^-, w^-)$.
2. If $\rho^- > \sigma(w^-)$, then ρ^+ must be in $\mathcal{N}(U^-) = [\sigma(w^-), \rho^{\max}]$.

The proof of the previous proposition is analogous to the one proposed in [17], where the authors study the Riemann problem on a network for the Aw-Rascle model, which belongs to the GSOM. In Figure 3 we show an example of the two possible states configurations at incoming road.

Remark 3.2. We observe that the flux of the right state satisfies

$$Q(\rho^+, w^+) \leq d(\rho^-, w^-), \quad (3.12)$$

where d is the demand function defined in (3.11). Indeed, if $\rho^- \leq \sigma(w^-)$ then ρ^+ must be in $\mathcal{N}(U^-) = [\tilde{\rho}^-(w^-), \rho^{\max}]$, where the flux is lower than or equal to $Q(\rho^-, w^-)$; if $\rho^- > \sigma(w^-)$, then ρ^+ must be in $\mathcal{N}(U^-) = [\sigma(w^-), \rho^{\max}]$, where the flux is lower than $Q^{\max}(w^-)$. These two possibilities are summarized in (3.12).

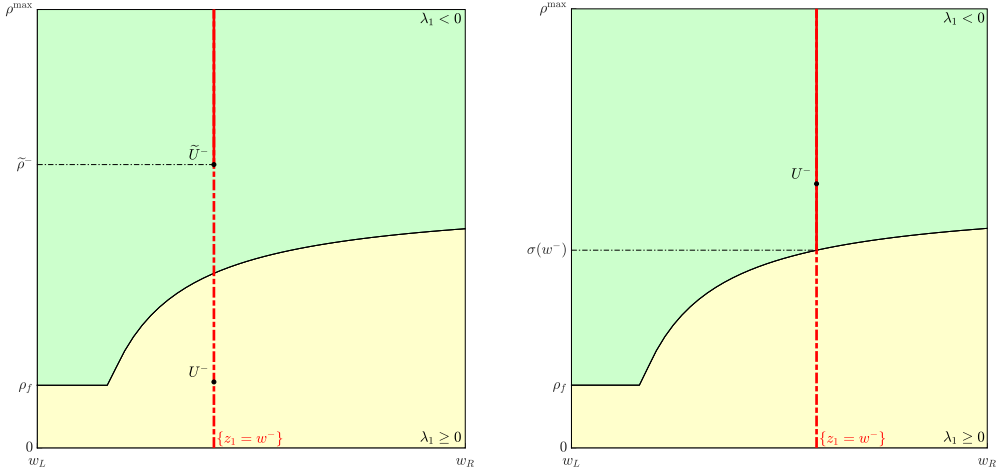


Figure 3. Two possible configurations of incoming road states. The red segment identifies the set of possible right states $U^+ = (\rho^+, w^+)$ reachable from the left state U^- .

3.2 Outgoing road at the junction

Let us consider an outgoing road at the junction. We are interested in the waves with non-negative speed, thus we can have a 1-shock or 1-rarefaction wave and a 2-contact discontinuity. Let us fix a right state $U^+ = (\rho^+, w^+)$, our aim is to define the set of all possible left states $U^- = (\rho^-, w^-)$ that can be connected to U^+ with waves with non-negative speed. We denote by $\mathcal{P}(U^+)$ the set of admissible densities.

Proposition 3.2. Let $U^+ = (\rho^+, w^+)$ be a right state on an outgoing road, and v^+ the associated velocity $V(\rho^+, w^+)$. Let $U^\dagger = (\rho^\dagger, w^\dagger)$ be the intersection point between the level curves $\{z_2 = v^+\}$ and $\{z_1 = c\}$, for a certain c , with $\rho^\dagger = \rho^\dagger(v^+, c)$ and $w^\dagger = c$. The set of possible left states $U^- = (\rho^-, w^-)$ that can be connected to the right state are such that $w^- = c$ and

1. If $\rho^\dagger \leq \sigma(w^+)$, then ρ^- must be in $\mathcal{P}(U^+) = [0, \sigma(w^\dagger)]$.
2. If $\rho^\dagger > \sigma(w^+)$, then ρ^- must be in $\mathcal{P}(U^+) = [0, \tilde{\rho}^\dagger(w^\dagger)] \cup \{\rho^\dagger\}$, where $\tilde{\rho}^\dagger(w^\dagger)$ is the density such that $Q(\tilde{\rho}^\dagger(w^\dagger), w^\dagger) = Q(\rho^\dagger, w^\dagger)$.

Again, we refer to [17] for the details of the proof. In Figure 4 we show an example of the two possible states configurations at outgoing road.

Remark 3.3. We observe that $w^\dagger = w^- = c$ and that the flux of the left state satisfies

$$Q(\rho^-, w^-) \leq s(\rho^\dagger, w^\dagger), \quad (3.13)$$

where s is the supply function defined in (3.10). Indeed, if $\rho^\dagger \leq \sigma(w^+)$ then ρ^- must be in $\mathcal{P}(U^+) = [0, \sigma(w^\dagger)]$, where the flux is lower than or equal to $Q^{\max}(w^\dagger)$; if $\rho^\dagger > \sigma(w^+)$, then ρ^- must be in $\mathcal{P}(U^+) = [0, \tilde{\rho}^\dagger(w^\dagger)] \cup \{\rho^\dagger\}$, where the flux is lower than $Q(\rho^\dagger, w^\dagger)$. These two possibilities are summarized in (3.13).

We focus now on the intersection point U^\dagger between the level curves of the two Riemann invariants $\{z_1 = w^-\}$ and $\{z_2 = v^+\}$, for a certain w^- and v^+ . In the propositions which follow, we refer to Figures 5 and 6, whose plots are obtained with the CGARZ model and flux functions defined in Section 5. However, the statements of Propositions 3.3 and 3.4 hold for any GSOM with flux and velocity functions satisfying properties (H1)-(H6).

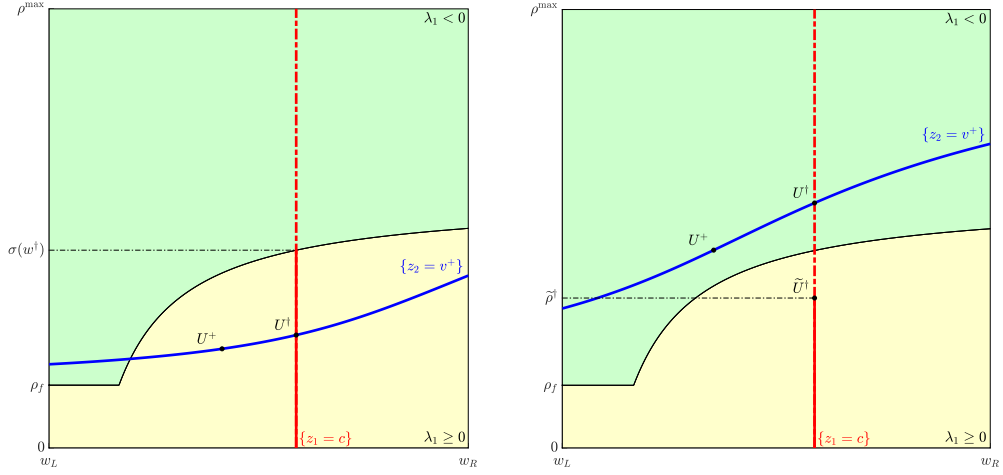


Figure 4. Two possible configurations of outgoing road. The red segment identifies the set of possible left states $U^- = (\rho^-, w^-)$ reachable from the left state U^+ .

Proposition 3.3. Let V be a velocity function verifying hypotheses (H5) and (H6), the following statements hold.

1. The intersection point $U^\dagger = (\rho^\dagger, w^\dagger)$ is such that $w^\dagger = w^-$ and $\rho^\dagger(v^-, w^-)$ is the unique density value such that $V(\rho^\dagger, w^-) = v^+$.
2. The function $\rho^\dagger(v^-, w)$ is non-decreasing in w .

Proof. We have $w^\dagger = w^-$ by construction, while the uniqueness of ρ^\dagger follows by the property (H5) of the velocity function V . To prove the monotonicity of ρ^\dagger , let us consider the family of speed functions $V(\rho, w)$ (see for example the left plot of Figure 5). If we cut the speed-family with a horizontal line $V = v^+$, we obtain the density values whose velocity is equal to v^+ as w changes. By property (H6) follows that ρ is non-decreasing in w , thus the level curve $\{z_2 = v^+\}$ is non-decreasing in the (w, ρ) -plane, see the right plot of Figure 5. Since ρ^\dagger lies on these curves the thesis follows.

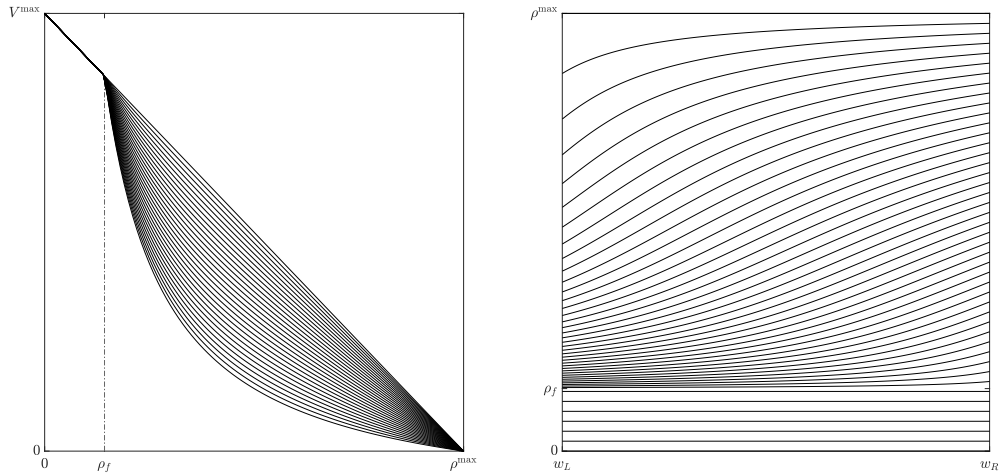


Figure 5. Example of family of speed functions (left) and level curves of ρ^\dagger for different values of v^+ (right).

□

Proposition 3.4. For any $v^+ \in [0, V^{\max}]$ and $w \in [w_L, w_R]$ the function $s(\rho^\dagger, w)$ (3.10) is non-decreasing in w , where $\rho^\dagger = \rho^\dagger(v^+, w)$ is the density of the intersection point between the level curves of the two Riemann invariants $\{z_1 = w\}$ and $\{z_2 = v^+\}$.

Proof. First of all we observe that all the points ρ^\dagger along the level curve $\{z_2 = v^+\}$ are such that $Q(\rho^\dagger, w) = v^+ \rho^\dagger$, for any $w \in [w_L, w_R]$. Since ρ^\dagger is non-decreasing in w by Proposition 3.3, also the flux along the curve is non-decreasing in w . We divide the proof in four cases.

1. The level curve $\{z_2 = v^+\}$ is entirely below the curve $\rho = \sigma(w)$, see Figure 6(a). In this case we have $s(\rho^\dagger, w) = Q^{\max}(w)$, which is non-decreasing in w by property (H3).
2. The level curve $\{z_2 = v^+\}$ has a unique intersection point with the curve $\rho = \sigma(w)$, see Figure 6(b). In this case, denoting by $U^* = (w^*, \rho^*)$ the intersection point, we have

$$s(\rho^\dagger, w) = \begin{cases} v^+ \rho^\dagger & \text{if } w \leq w^* \\ Q^{\max}(w) & \text{if } w > w^*, \end{cases}$$

which is non-decreasing in w by Proposition 3.3 and property (H3).

3. The level curve $\{z_2 = v^+\}$ has two intersection points with the curve $\rho = \sigma(w)$, see Figure 6(c). We denote by $\bar{U} = (\bar{w}, \bar{\rho})$ and $U^* = (w^*, \rho^*)$ the first and the second intersection point, respectively. We have

$$s(\rho^\dagger, w) = \begin{cases} v^+ \rho^\dagger & \text{if } w \leq \bar{w} \\ Q^{\max}(w) & \text{if } \bar{w} < w \leq w^* \\ v^+ \rho^\dagger & \text{if } w > w^*. \end{cases}$$

We observe that we recover the previous case for the points $U = (w, \rho)$ such that $w \leq w^*$. Since U^* intersects $\sigma(w)$, we have $Q(\rho^*, w^*) = Q^{\max}(w^*) = v^+ \rho^*$. For any $\delta, \varepsilon > 0$, if $(w + \delta, \rho^* + \varepsilon) \in \{z_2 = v^+\}$ then $Q(\rho^* + \varepsilon, w^* + \delta) = v^+(\rho^* + \varepsilon) > Q(\rho^*, w^*)$, thus the supply function is always non-decreasing also for $w > w^*$.

4. The level curve $\{z_2 = v^+\}$ is entirely above the curve $\rho = \sigma(w)$, see Figure 6(d). In this case we have $s(\rho^\dagger, w) = v^+ \rho^\dagger$, which is non-decreasing in w by Proposition 3.3.

□

4 The GSOM on networks

In this work we deal with road networks characterized by simple junctions. Specifically, we define the solution for junctions with one incoming road and one outgoing road, one incoming road and two outgoing roads and two incoming roads and one outgoing road.

4.1 One incoming and one outgoing road at junction

We consider the simplest case of two roads connected by a junction. We have a left state U_1^- for the incoming road and a right state U_2^+ for the outgoing road and we have to solve the Riemann problem at the junction. Thus, our aim is to recover U_1^+ and U_2^- .

We assume that ρ and y are conserved at the junction, i.e.

$$\rho_1^+ v_1^+ = \rho_2^- v_2^- \quad (4.1)$$

$$\rho_1^+ v_1^+ w_1^+ = \rho_2^- v_2^- w_2^-. \quad (4.2)$$

Equation (4.1) implies that $q_1^+ = q_2^-$, therefore equation (4.2) implies $w_1^+ = w_2^-$. Since w is the first Riemann invariant, by the preliminary studies on the incoming road we have $w_1^- = w_1^+ = w_2^-$. This

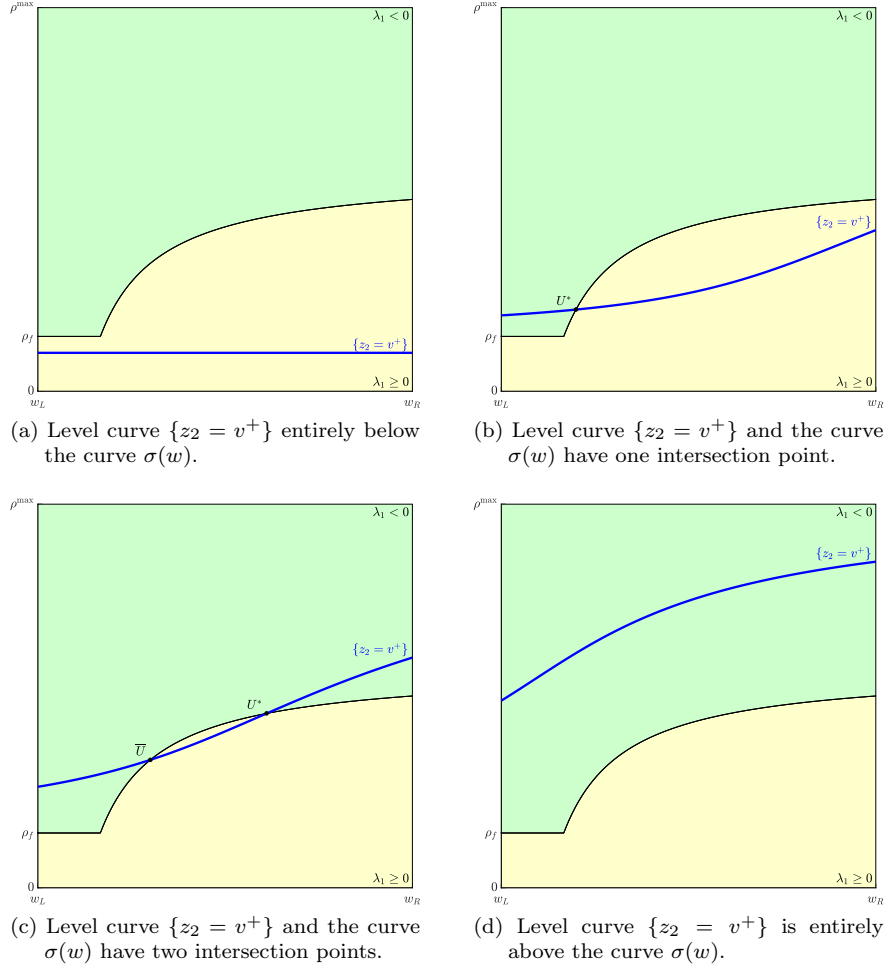


Figure 6. Four possible cases of the position of the level curve $\{z_2 = v^+\}$ with respect to the curve $\rho = \sigma(w)$.

means that U_1^+ and U_2^- must lay along the level curve $\{z_1 = w_1^-\}$. Thus the point $U_2^\dagger = (\rho_2^\dagger, w_2^\dagger)$ of the outgoing road is defined by the intersection between $\{z_1 = w_1^-\}$ and the level curve $\{z_2 = v_2^+\}$ passing through U_2^+ , where $v_2^+ = V(\rho_2^+, w_2^+)$. This means that $w_2^\dagger = w_2^- = w_1^-$.

In order to define a unique solution, we look for the one which maximizes the flux. By Remarks 3.2 and 3.3, we have to solve the following maximization problem

$$\begin{aligned} & \max q \text{ subject to} \\ & 0 \leq q \leq d(\rho_1^-, w_1^-) \\ & 0 \leq q \leq s(\rho_2^\dagger, w_1^-), \end{aligned} \tag{4.3}$$

which is equivalent to $\bar{q} = \min\{d(\rho_1^-, w_1^-), s(\rho_2^\dagger, w_1^-)\}$. Thus, $q_1^+ = q_2^- = \bar{q}$. Once q_1^+ and q_2^- are known, we define $\rho_1^+ \in \mathcal{N}(U_1^-)$ such that $Q(\rho_1^+, w_1^+) = q_1^+$, and $\rho_2^- \in \mathcal{P}(U_2^+)$ such that $Q(\rho_2^-, w_2^-) = q_2^-$.

Example 1. In Figure 7 we show an example of a junction with one incoming and one outgoing road. Following the procedure above described, we have $w_1^+ = w_2^- = w_2^\dagger = w_1^-$, $\mathcal{N}(U_1^-) = [\tilde{\rho}_1^-(w_1^-), \rho^{\max}]$, $\mathcal{P}(U_2^+) = [0, \tilde{\rho}_2^+(w_2^+)] \cup \{\rho_2^\dagger\}$ and $\bar{q} = Q(\rho_2^\dagger, w_1^-)$. Therefore the points U_1^+ and U_2^- coincide and are defined by

$$U_1^+ = U_2^- = (\rho_2^\dagger, w_1^-).$$

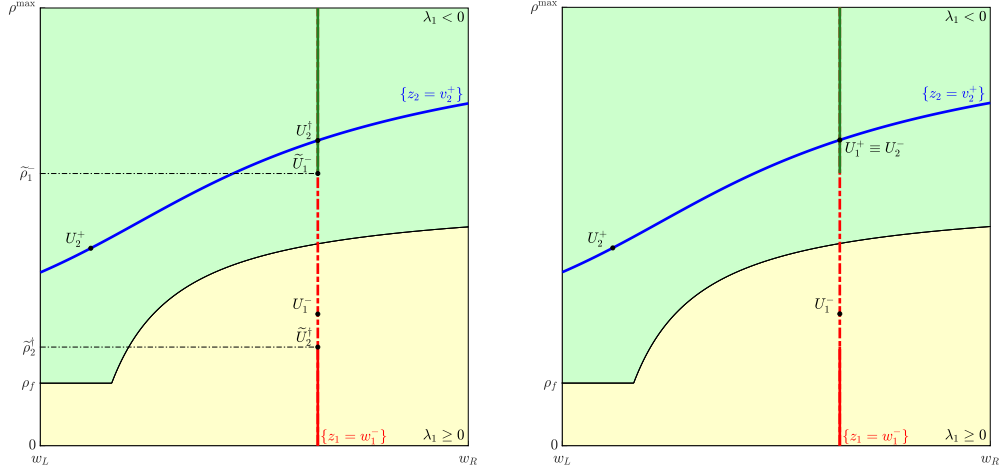


Figure 7. Example of $1 \rightarrow 1$ junction: the procedure to follow (left) and the solution (right). The green segment along $\{z_1 = w_1^-\}$ is $\mathcal{N}(U_1^-)$, the red segment is $\mathcal{P}(U_2^+)$.

4.2 Diverge junction

We consider the case of one incoming road and two outgoing roads at junction. We have a left state U_1^- for the incoming road and two right states U_2^+ and U_3^+ for the outgoing roads and our aim is to recover U_1^+ , U_2^- and U_3^- . We introduce the parameter $\alpha \in (0, 1)$ which defines how vehicles distribute from the incoming road to the outgoing roads. Indeed, vehicles are distributed in proportion α and $1 - \alpha$ on the roads 2 and 3 respectively. Again, we assume the conservation of ρ and y , thus we have

$$\alpha \rho_1^+ v_1^+ = \rho_2^- v_2^- \quad (4.4)$$

$$\alpha \rho_1^+ v_1^+ w_1^+ = \rho_2^- v_2^- w_2^- \quad (4.5)$$

$$(1 - \alpha) \rho_1^+ v_1^+ = \rho_3^- v_3^- \quad (4.6)$$

$$(1 - \alpha) \rho_1^+ v_1^+ w_1^+ = \rho_3^- v_3^- w_3^- \quad (4.7)$$

Equation (4.4) in (4.5) implies $w_1^+ = w_2^-$. Analogously, equation (4.6) in (4.7) implies $w_1^+ = w_3^-$. As in Section 4.1, we have $w_1^- = w_1^+$ hence $w_2^- = w_3^- = w_1^-$. Thus, the two intersection points U_2^\dagger and U_3^\dagger between the two level curves of the second Riemann invariant passing through U_2^+ and U_3^+ are defined by their intersection with the level curve $\{z_1 = w_1^-\}$, i.e. $w_2^\dagger = w_3^\dagger = w_1^-$ while ρ_2^\dagger and ρ_3^\dagger depend on $V(\rho_2^\dagger, w_1^-) = v_2^+$ and $V(\rho_3^\dagger, w_1^-) = v_3^+$, respectively.

In this case, in order to define a unique solution, we have to solve the following maximization problem

$$\begin{aligned} & \max q \text{ subject to} \\ & 0 \leq q \leq d(\rho_1^-, w_1^-) \\ & 0 \leq \alpha q \leq s(\rho_2^\dagger, w_1^-) \\ & 0 \leq (1 - \alpha)q \leq s(\rho_3^\dagger, w_1^-), \end{aligned} \quad (4.8)$$

which leads us to $\bar{q} = \min\{d(\rho_1^-, w_1^-), s(\rho_2^\dagger, w_1^-)/\alpha, s(\rho_3^\dagger, w_1^-)/(1 - \alpha)\}$. Once \bar{q} is found we have

$$\begin{aligned} q_1^+ &= \bar{q} \\ q_2^- &= \alpha \bar{q} \\ q_3^- &= (1 - \alpha) \bar{q}, \end{aligned}$$

and then we define $\rho_1^+ \in \mathcal{N}(U_1^-)$ such that $Q(\rho_1^+, w_1^+) = q_1^+$, $\rho_2^- \in \mathcal{P}(U_2^+)$ such that $Q(\rho_2^-, w_2^-) = q_2^-$ and $\rho_3^- \in \mathcal{P}(U_3^+)$ such that $Q(\rho_3^-, w_3^-) = q_3^-$.

Example 2. In Figure 8 we show an example of a junction with one incoming and two outgoing roads. Following the procedure above described, we have $w_1^+ = w_2^- = w_3^- = w_2^+ = w_3^+ = w_1^-$, $\mathcal{N}(U_1^-) = [\tilde{\rho}_1^-(w_1^-), \rho^{\max}]$, $\mathcal{P}(U_2^+) = [0, \tilde{\rho}_2^+(w_2^+)]$, $\mathcal{P}(U_3^+) = [0, \sigma(w_1^-)]$. We fix $\alpha = 0.7$ and then we have $\bar{q} = Q(\rho_1^-, w_1^-)$. Therefore $\rho_1^+ = \tilde{\rho}_1^-(w_1^-)$, while ρ_2^- and ρ_3^- are defined by

$$Q(\rho_2^-, w_1^-) = 0.7\bar{q} \quad \text{and} \quad Q(\rho_3^-, w_1^-) = (1 - 0.7)\bar{q}.$$

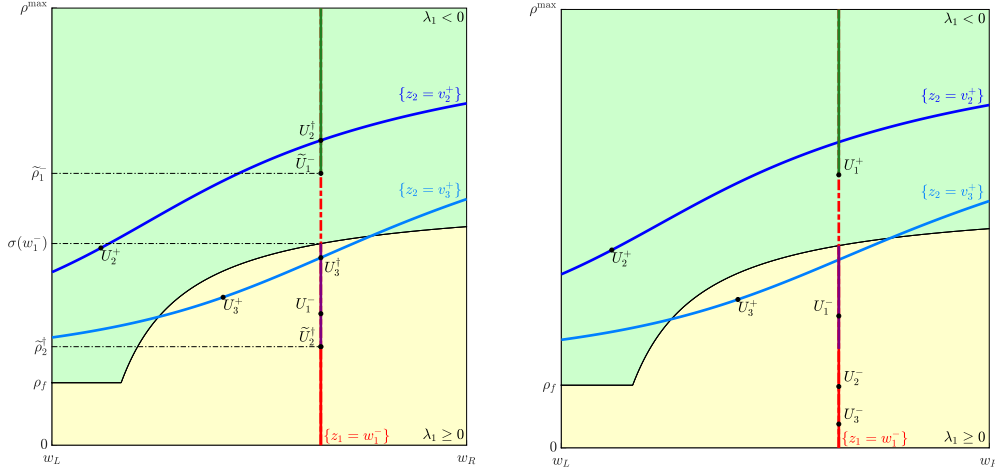


Figure 8. Example of $1 \rightarrow 2$ junction: the procedure to follow (left) and the solution (right). The green segment along $\{z_1 = w_1^-\}$ is $\mathcal{N}(U_1^-)$, the red segment is $\mathcal{P}(U_2^+)$ and the red segment combined with the purple one is $\mathcal{P}(U_3^+)$.

4.3 Merge junction

We consider the case of two incoming roads and one outgoing road at junction. We have two left states U_1^- and U_2^- for the incoming roads and a right state U_3^+ for the outgoing road and our aim is to recover U_1^+ , U_2^+ and U_3^- . We assume that vehicles from roads 1 and 2 enter into the road 3 with respect to the following priority rule

$$q_2^+ = \frac{\beta}{1 - \beta} q_1^+ \quad (4.9)$$

where β is a parameter in $[0, 1]$. Moreover we assume the conservation of ρ and y at junction, i.e.

$$\rho_1^+ v_1^+ + \rho_2^+ v_2^+ = \rho_3^- v_3^- \quad (4.10)$$

$$\rho_1^+ v_1^+ w_1^+ + \rho_2^+ v_2^+ w_2^+ = \rho_3^- v_3^- w_3^-. \quad (4.11)$$

Equation (4.10) implies $q_1^+ + q_2^+ = q_3^-$ and this identity, combined with (4.9) in (4.11) implies

$$w_3^- = (1 - \beta)w_1^+ + \beta w_2^+. \quad (4.12)$$

Since the first Riemann invariant is w , we have $w_1^+ = w_1^-$ and $w_2^+ = w_2^-$. Hence, it remains to compute the values q_1^+ , q_2^+ , q_3^- and w_3^- . Relations (4.9)-(4.12) fix some of them and we have to define the remaining free variables. We then move to the (q_1, q_2) -plane and we look for the maximization of the

flow. Therefore, we introduce $d_1 = d(\rho_1^-, w_1^-)$, $d_2 = d(\rho_2^-, w_2^-)$ and the rectangle $\Omega = [0, d_1] \times [0, d_2]$, and we focus on the intersection point between the straight lines

$$r : q_2 = \frac{\beta}{1 - \beta} q_1 \quad (4.13)$$

$$s : q_2 = s_3 - q_1, \quad (4.14)$$

where $s_3 = s(\rho_3^\dagger, w_3^-)$. Note that $s_3 = s_3(\beta)$, since both ρ_3^\dagger and w_3^- depend on β . The intersection point is

$$P = ((1 - \beta)s_3, \beta s_3). \quad (4.15)$$

In the following we define U_1^+ , U_2^+ and U_3^- .

Definition 4.1. Assuming (4.10) and (4.12) we define first the two values q_1^+ and q_2^+ which depend on the position of the intersection point P and then the other variables.

i. Procedure to set the incoming fluxes q_1^+ and q_2^+ .

1. The point P is inside the rectangle, i.e.

$$\begin{cases} (1 - \beta)s_3 \leq d_1 \\ \beta s_3 \leq d_2, \end{cases}$$

see Figure 9(a). In this case the point P identifies $q_1^+ = (1 - \beta)s_3$ and $q_2^+ = \beta s_3$.

2. The point P is to the right of the rectangle, i.e.

$$\begin{cases} (1 - \beta)s_3 > d_1 \\ \beta s_3 \leq d_2, \end{cases}$$

see Figure 9(b). We have the following possibilities:

- (a) If we need to respect the priority rule, then the incoming fluxes must be on the straight line r , thus the point Q in Figure 9(b) identifies $q_1^+ = d_1$ and $q_2^+ = \beta d_1 / (1 - \beta)$.
- (b) If there exists a $\tilde{\beta} > \beta$ such that the intersection point between the corresponding straight lines r and s crosses the rectangle in d_1 , as the point R in Figure 9(b), then that point defines $q_1^+ = d_1$, $q_2^+ = \tilde{\beta} s_3(\tilde{\beta})$ and $w_3^- = (1 - \tilde{\beta})w_1^- + \tilde{\beta}w_2^-$. Otherwise the point S in Figure 9(b) identifies $q_1^+ = d_1$, $q_2^+ = d_2$ and $w_3^- = (1 - \tilde{\beta})w_1^- + \tilde{\beta}w_2^-$, where $\tilde{\beta} = d_2 / (d_1 + d_2)$.

3. The point P is above the rectangle, i.e.

$$\begin{cases} (1 - \beta)s_3 \leq d_1 \\ \beta s_3 > d_2. \end{cases}$$

see Figure 9(c). We have the following possibilities:

- (a) If we need to respect the priority rule, then the incoming fluxes must be on the straight line r , thus the point Q in Figure 9(c) identifies $q_1^+ = (1 - \beta)d_2 / \beta$ and $q_2^+ = d_2$.
- (b) If there exists a $\tilde{\beta} < \beta$ such that the intersection point between the corresponding straight lines r and s crosses the rectangle in d_2 , as the point R in Figure 9(c), then that point defines $q_1^+ = (1 - \tilde{\beta})s_3(\tilde{\beta})$, $q_2^+ = d_2$ and $w_3^- = (1 - \tilde{\beta})w_1^- + \tilde{\beta}w_2^-$. Otherwise the point S in Figure 9(c) identifies $q_1^+ = d_1$, $q_2^+ = d_2$ and $w_3^- = (1 - \tilde{\beta})w_1^- + \tilde{\beta}w_2^-$, where $\tilde{\beta} = d_2 / (d_1 + d_2)$.

4. The point P is completely outside the rectangle, i.e.

$$\begin{cases} (1 - \beta)s_3 > d_1 \\ \beta s_3 > d_2, \end{cases}$$

see Figure 9(d). In this case, if we need to respect the priority rule we recover the case 2(a) or 3(a), depending on β . Otherwise we recover the case 2(b) or 3(b), depending on β .

- ii. We obtain $q_3^- = q_1^+ + q_2^+$ and we define $\rho_1^+ \in \mathcal{N}(U_1^-)$ such that $Q(\rho_1^+, w_1^+) = q_1^+$, $\rho_2^+ \in \mathcal{N}(U_2^-)$ such that $Q(\rho_2^+, w_2^+) = q_2^+$ and $\rho_3^- \in \mathcal{P}(U_3^+)$ such that $Q(\rho_3^-, w_3^-) = q_3^-$.

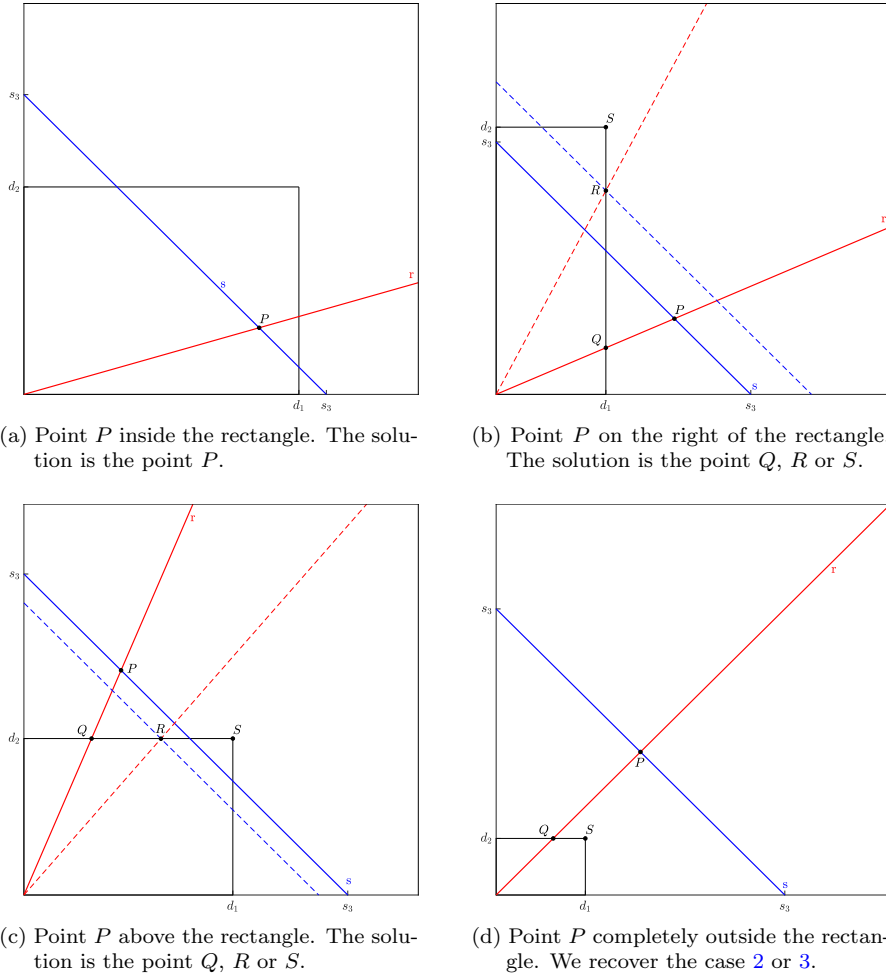


Figure 9. The four possible positions of the point P with respect to the rectangle Ω .

Proposition 4.1. The values U_1^+ , U_2^+ and U_3^- given in Definition 4.1 are uniquely defined.

Proof. We have that the angle between the straight line r and the x -axis of the (q_1, q_2) -plane always increases with β . The straight line s , instead, moves to the bottom if $w_1^- > w_2^-$ and to the top if $w_1^- \leq w_2^-$. Indeed, in the first case w_3^- decreases with β and, as consequence of Proposition 3.4, s_3 is non-increasing, while in the second case w_3^- increases with β and s_3 is non-decreasing.

Therefore, by the monotonicity of s_3 the procedure described above identifies a unique couple of values (q_1^+, q_2^+) and consequently the solution U_1^+ , U_2^+ and U_3^- is uniquely defined. \square

Example 3. In Figure 10 we show an example of a junction with two incoming and one outgoing roads. Following the procedure above described, we fix $\beta = 0.6$ and we have $w_1^+ = w_1^-$, $w_2^+ = w_2^-$, $w_3^+ = (1 - \beta)w_1^- + \beta w_2^-$, $\mathcal{N}(U_1^-) = [\sigma(\rho_1^-), \rho^{\max}]$, $\mathcal{N}(U_2^-) = [\tilde{\rho}_2^+(w_2^-), \rho^{\max}]$, $\mathcal{P}(U_3^+) = [0, \sigma(w_3^-)]$. The point P of intersection between the straight lines r and s is inside the rectangle Ω , thus $q_1^+ = (1 - \beta)s_3(\beta)$, $q_2^+ = \beta s_3(\beta)$ and $q_3^- = s_3(\beta)$. Finally we compute the densities ρ_1^+ , ρ_2^+ and ρ_3^- such that $q_1^+ = Q(\rho_1^+, w_1^+)$, $q_2^+ = Q(\rho_2^+, w_2^+)$ and $q_3^- = Q(\rho_3^-, w_3^-)$, as shown in the right plot of Figure 10.

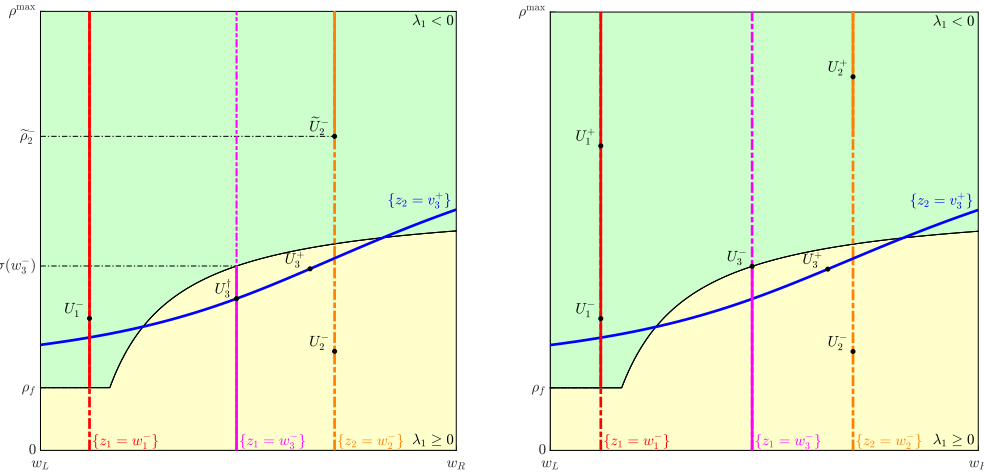


Figure 10. Example of 2 \rightarrow 1 junction: the procedure to follow (left) and the solution (right).

Remark 4.1. The solution proposed in [17] can be recovered by fixing $\beta = 0.5$ in our procedure.

Remark 4.2. Let us consider the particular case of w constant in all the roads. The 1 \rightarrow 1 and 1 \rightarrow 2 junctions can be treated exactly as the LWR model at junction, as done in [14]. For the 2 \rightarrow 1 junction we observe that the assumption of w constant implies that the straight line s defined in (4.14) coincides for all β , therefore the solution is limited to the points P or Q , excluding the points R or S . Thus, we recover again the LWR model on networks, as treated in [14].

5 Numerical simulations

In this section we show some numerical tests to simulate the solution for different types of junction. We consider the traffic model on a network with roads $I_r = [a_r, b_r]$ during a time interval $[0, T]$. We divide each road into $N_x + 1$ cells of length Δx , and the time interval into $N_t + 1$ steps of length Δt . We choose the CGARZ model among the family of GSOM, which is numerically solved with the 2CTM scheme [11] with suitable boundary conditions on the cells which are at the extremes of the network. Depending on the type of junction we use the theory defined in Sections 4.1, 4.2 and 4.3 to compute the density and the property of vehicles w on the junction boundary cells, which are denoted by ρ_r^J and w_r^J respectively, for each road r .

The CGARZ model assumes that flux of vehicles is not influenced by w when the density value is lower than a certain threshold. Thus, the flux of the CGARZ model is described by a single-valued fundamental diagram in free-flow regimes, and by a multi-valued function in congestion. The flux

function is then defined by

$$Q(\rho, w) = \begin{cases} Q_f(\rho) & \text{if } 0 \leq \rho \leq \rho_f \\ Q_c(\rho, w) & \text{if } \rho_f < \rho \leq \rho^{\max}, \end{cases} \quad (5.1)$$

where ρ_f is the *free-flow threshold density* and ρ^{\max} is the maximum density. Following [4], we assume that the flux function is described by the Greenshields model in the free-flow phase, i.e.

$$Q_f(\rho) = \frac{V^{\max}}{\rho^{\max}} \rho (\rho^{\max} - \rho), \quad (5.2)$$

and by a convex combination of a lower-bound function $f(\rho)$ and an upper-bound function $g(\rho)$ in the congested phase. In particular, we set

$$f(\rho) = \frac{V^{\max}}{\rho^{\max}} \rho_f (\rho^{\max} - \rho) \quad (5.3)$$

$$g(\rho) = \frac{V^{\max}}{\rho^{\max}} \rho (\rho^{\max} - \rho). \quad (5.4)$$

We define

$$\theta(w) = \frac{w - w_L}{w_R - w_L}, \quad (5.5)$$

with $w_L = Q_f(\rho_f)$ and $w_R = Q_f(\rho^{\max}/2)$, where $\rho^{\max}/2$ is the critical density of $Q_f(\cdot)$. Note that this means that w identifies the maximum reachable flux by the flux function.

The flux function in the congested phase $Q_c(\rho, w)$ is then defined by

$$Q_c(\rho, w) = (1 - \theta(w))f(\rho) + \theta(w)g(\rho), \quad (5.6)$$

with f and g given in (5.3) and (5.4). The velocity function is

$$V(\rho, w) = \frac{Q(\rho, w)}{\rho}. \quad (5.7)$$

In all the tests which follow we fix these parameters: $\rho_f = 19$ veh/km, $\rho^{\max} = 133$ veh/km, $V^{\max} = 120$ km/h, $L = 1$ km, $T = 2$ min, $\Delta x = 0.02$ km, $\Delta t = 0.3$ s, $w_L = 1954$ and $w_R = 3990$.

5.1 The case of 1 \rightarrow 1 junction

Let us consider two roads connected by a junction, as depicted in Figure 11. We denote by $\rho_{1,j}^n = \rho_1(x_j, t^n)$ the density of road 1, and by $\rho_{2,j}^n = \rho_2(x_j, t^n)$ the density of road 2, for $j = 0, \dots, N_x$ and $n = 0, \dots, N_t$. We use the 2CTM scheme to compute the density on the nodes inside the roads, i.e. $\rho_{1,j}^n$ for $j = 0, \dots, N_x - 1$ and $\rho_{2,j}^n$ for $j = 1, \dots, N_x$. The junction is treated as a boundary ghost cell and densities $\rho_{1,N_x}^n = \rho_1^J$ and $\rho_{2,0}^n = \rho_2^J$ are computed as explained in Section 4.1.

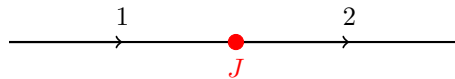


Figure 11. Example of 1 \rightarrow 1 junction.

In the following test the couple $(\rho_{r,\cdot}^0, w_{r,\cdot}^0)$ of the two roads is taken as in Table 1. The density at the left boundary of road 1 is fixed to $\rho_{1,0}^0 = 50$ veh/km for any time and the right boundary of road 2 is such that vehicles are free to leave the road. Figure 12 shows the evolution of traffic in time. At the beginning the dynamic of the first road is described by a shock wave which moves backwards until it moves to a rarefaction wave, while the vehicles enter into the second road with a rarefaction wave. Note that, the dynamic of road 2 is slowed down by its lower value of w with respect to road 1, which imposes vehicles to have a slower velocity.

Road r	$\rho_{r,j}^0$ (veh/km)	$w_{r,\cdot}^0$
1	$50 \quad j \leq N_x/2$ $100 \quad j > N_x/2$	w_R
2	$70 \quad \forall j$	w_L

Table 1. Initial data for the $1 \rightarrow 1$ junction.

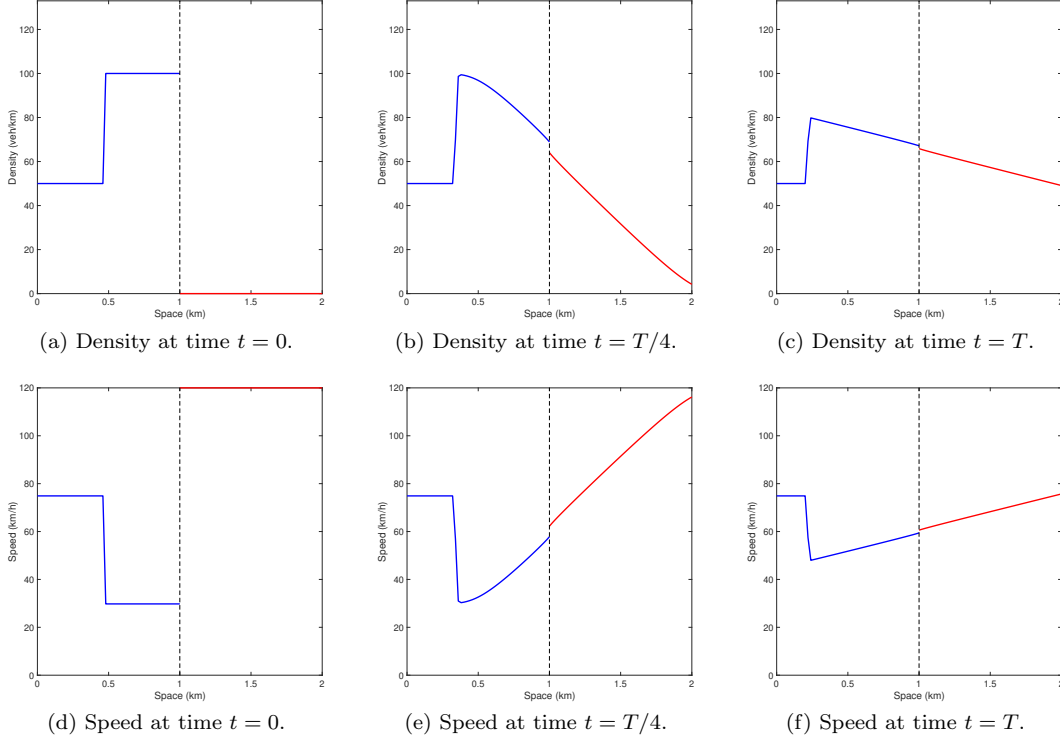


Figure 12. Junction $1 \rightarrow 1$: plot of density (top) and speed (bottom) of vehicles at different times.

5.2 The case of $1 \rightarrow 2$ junction

Let us consider a junction with one incoming road and two outgoing roads, depicted in Figure 13. The density of roads 1, 2 and 3 is computed with the 2CTM scheme inside the roads. We solve the Riemann problem at junction as described in Section 4.2 to obtain $\rho_{1,N_x}^n = \rho_1^J$, $\rho_{2,0}^n = \rho_2^J$ and $\rho_{3,0}^n = \rho_3^J$, for $n = 0, \dots, N_t$.

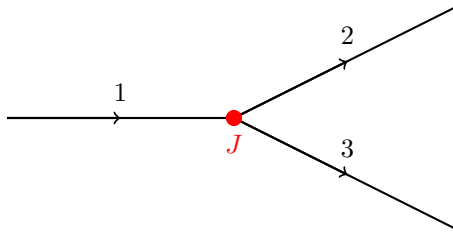


Figure 13. Example of $1 \rightarrow 2$ junction.

We simulate two different scenarios, with the initial data shown in Table 2. The parameter α which defines how vehicles from road 1 distribute in roads 2 and 3 is $\alpha = 0.7$. Moreover, the left boundary density of road 1 is $\rho_{1,0}^n = 70$ veh/km for any time and the right boundary of road 2 and 3 is such that vehicles are free to leave the road. In Figures 14 and 15 we show the results of the two tests. The top plots show the density of vehicles at different times, while the bottom plots show their speed. The first difference between the two tests is the initial speed of vehicles: in Figure 14(d) road 1 and 2 have same density but different w and thus different speed, while in Figure 15(d) the two roads have also the same speed. Moreover, the lower value of w of road 2 in the first test generates a small queue on the first road, which is not created in the second test. At the end of the simulation, the density of road 3 is enough low to reduce the density of road 1 too. Note that the second test corresponds to what we would obtain with the LWR model on a network.

Test 1			Test 2		
Road r	$\rho_{r,\cdot}^0$ (veh/km)	$w_{r,\cdot}^0$	Road r	$\rho_{r,\cdot}^0$ (veh/km)	$w_{r,\cdot}^0$
1	70	w_R	1	70	w_R
2	70	w_L	2	70	w_R
3	5	$(w_R + w_L)/2$	3	5	w_R

Table 2. Initial data for the $1 \rightarrow 2$ junction: data of Test 1 on the left and of Test 2 on the right.

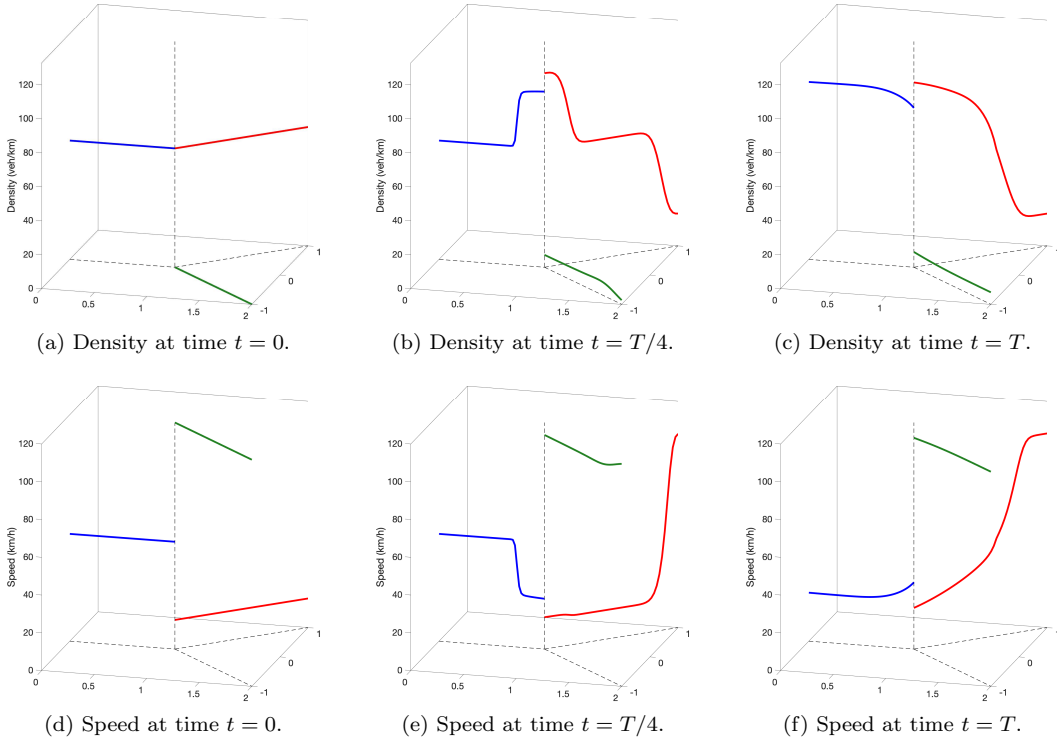


Figure 14. Test 1 junction $1 \rightarrow 2$: 3D plot of density (top) and speed (bottom) of vehicles at different times.

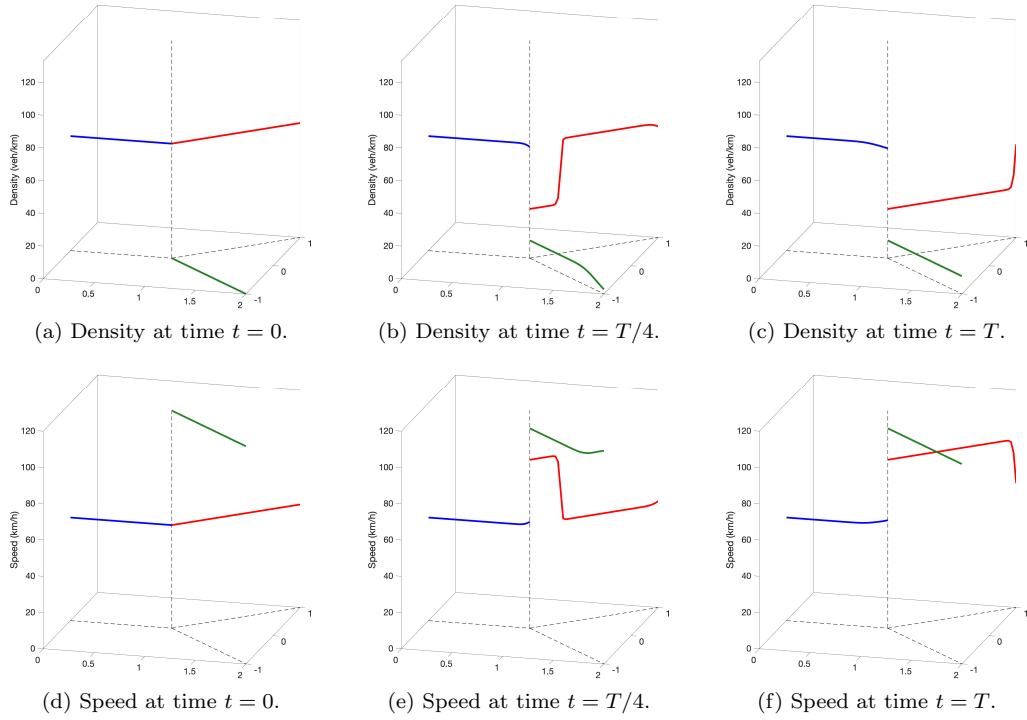


Figure 15. Test 2 junction 1 \rightarrow 2: 3D plot of density (top) and speed (bottom) of vehicles at different times.

5.3 The case of 2 \rightarrow 1 junction

Let us consider a junction with two incoming roads and one outgoing road, depicted in Figure 16. The density of roads 1, 2 and 3 is computed with the 2CTM scheme on the cells outside the junction. We solve the Riemann problem at junction as described in Section 4.3 to obtain $\rho_{1,N_x}^n = \rho_1^J$, $\rho_{2,N_x}^n = \rho_2^J$ and $\rho_{3,0}^n = \rho_3^J$, for $n = 0, \dots, N_t$.

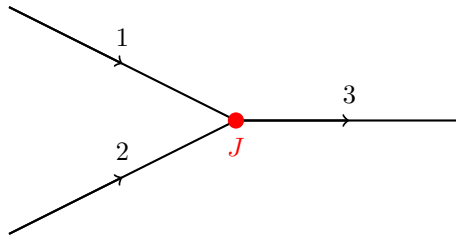


Figure 16. Example of 2 \rightarrow 1 junction.

We simulate two different scenarios with the initial data taken as in Table 3. The parameter β which defines the priority rule is fixed as $\beta = 0.6$. In road 1 vehicles continues to enter with density equal to 40 veh/km, no more vehicles enter into road 2 and the right boundary of road 3 is such that vehicles are free to leave the road. Finally, we observe that in both the tests we allow vehicles to not respect the priority rule. The test in Figure 17 shows that the lower value of w on road 2 is such that vehicles slowly reach the junction, while road 1 fills up quickly. Once road 2 is empty, all vehicles of road 1 move to road 3. The test in Figure 18, instead, starts with all the roads with same w . In this case vehicles of both roads 1 and 2 reach quickly the junction and thus road 2 empties more quickly

with respect to test 1.

Test 1			Test 2		
Road r	$\rho_{r,\cdot}^0$ (veh/km)	$w_{r,\cdot}^0$	Road r	$\rho_{r,\cdot}^0$ (veh/km)	$w_{r,\cdot}^0$
1	40	w_R	1	40	w_R
2	30	w_L	2	30	w_R
3	10	$(w_R + w_L)/2$	3	10	w_R

Table 3. Initial data for the $2 \rightarrow 1$ junction: data of Test 1 on the left and of Test 2 on the right.

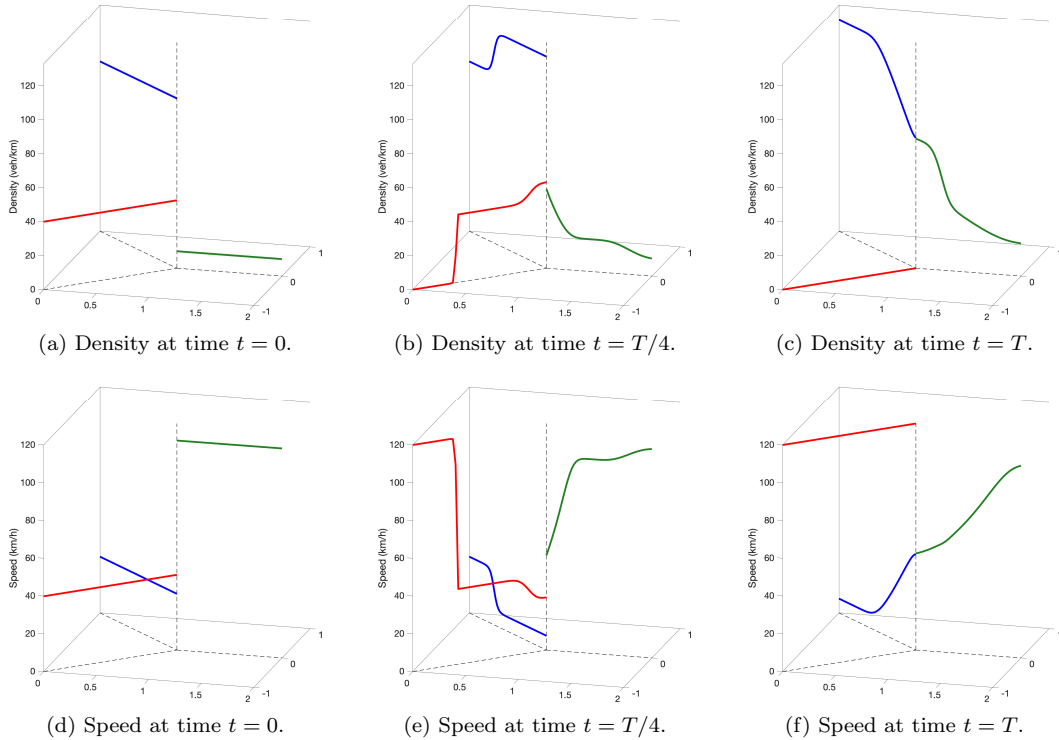


Figure 17. Test 1 junction $2 \rightarrow 1$: 3D plot of density (top) and speed (bottom) of vehicles at different times.

5.4 The case of a roundabout

Let us consider the roundabout depicted in Figure 19. We have four junctions: J_1 and J_3 of type $2 \rightarrow 1$, involving roads 1 and 8 into road 2 and roads 4 and 5 into road 6, respectively, and J_2 and J_4 of type $1 \rightarrow 2$, involving road 2 into roads 3 and 4 and road 6 into roads 7 and 8, respectively.

We treat junctions J_1 and J_3 as explained in Section 5.3 and junctions J_2 and J_4 as in Section 5.2. Vehicles enter into roads 1 and 5 with constant rate and roads 3 and 7 are such that vehicles are free to leave the network. The parameter α , which defines the distribution of vehicles for the $1 \rightarrow 2$ junction is $\alpha = 0.6$. In order to promote the motion on the roundabout, we define the parameter $\beta = 2/3$ for the junction J_1 and $\beta = 1/3$ for the junction J_3 . With this choices of β the dynamic favors the flux of vehicles from road 8 more than road 1, and from road 4 more than road 5. We test two scenarios: the congestion and the decongestion of the roundabout.

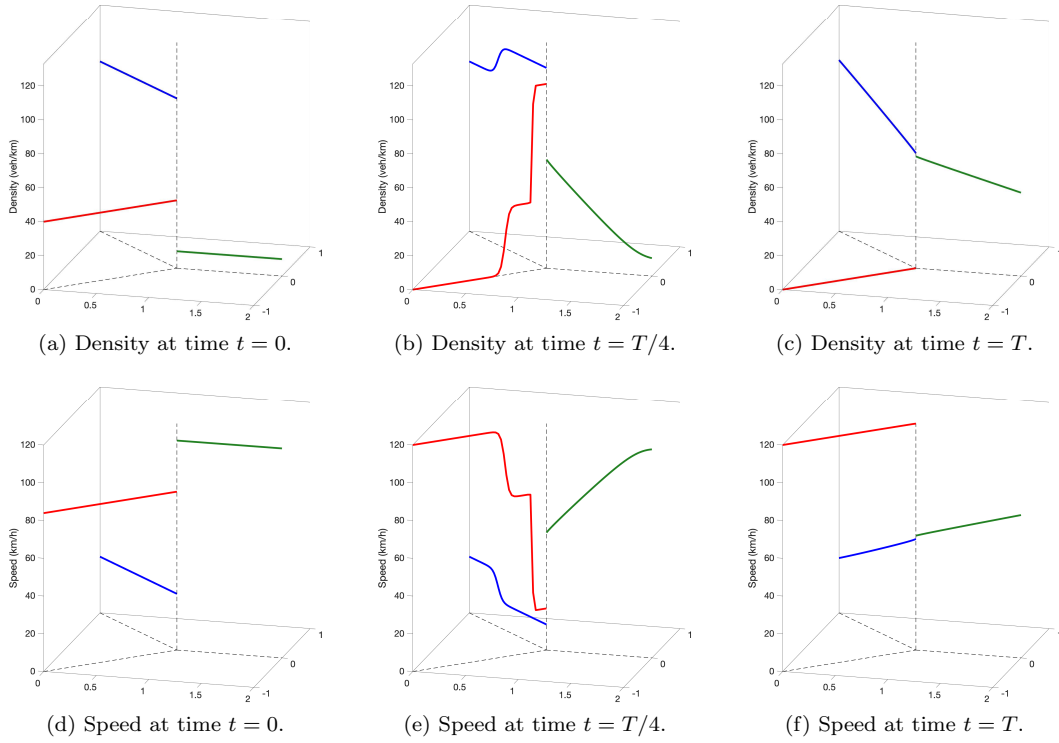


Figure 18. Test 2 junction $2 \rightarrow 1$: 3D plot of density (top) and speed (bottom) of vehicles at different times.

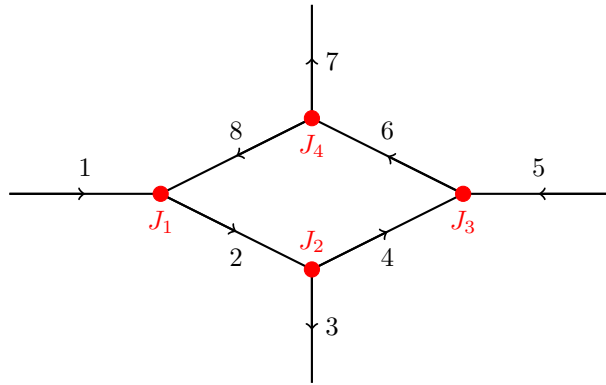


Figure 19. Example of roundabout.

The first test is the congestion of the roundabout starting from the initial data of the left panel of Table 4. With these initial data, vehicles enter into the roundabout with a higher flux from junction J_1 with respect to junction J_3 , where the value of w is lower. Indeed, the speed of vehicles is higher in road 1 than road 5. As a consequence, road 2 fills up more quickly than road 6. The dynamic of road 3, 4, 7 and 8 is quite similar. At the end of the simulation the dynamic reaches a sort of equilibrium, with higher density values on roads 1, 2, 3 and 4 with respect to roads 5, 6, 7 and 8.

To better analyze the dynamic of the roundabout, we focus on the four junctions. In Figure 21, we show how the boundary values (ρ^J, w^J) vary in time. In Figure 21(a) we see that, during the first minute of simulation, all vehicles from road 1 enter into road 2 (blue-circle and black-diamond

Test 1: congestion of roundabout			Test 2: decongestion of roundabout		
Road r	$\rho_{r,\cdot}^0$ (veh/km)	$w_{r,\cdot}^0$	Road r	$\rho_{r,\cdot}^0$ (veh/km)	$w_{r,\cdot}^0$
1	50	w_R	1	0	w_R
2	0	$(w_R + w_L)/2$	2	70	$(w_R + w_L)/2$
3	0	w_R	3	0	w_R
4	0	$(w_R + w_L)/2$	4	50	$(w_R + w_L)/2$
5	50	$(w_R + w_L)/2$	5	0	$(w_R + w_L)/2$
6	0	w_L	6	70	w_L
7	0	w_R	7	50	w_R
8	0	$(w_R + w_L)/2$	8	0	$(w_R + w_L)/2$

Table 4. Initial data for the roundabout: data of Test 1 on the left and of Test 2 on the right.

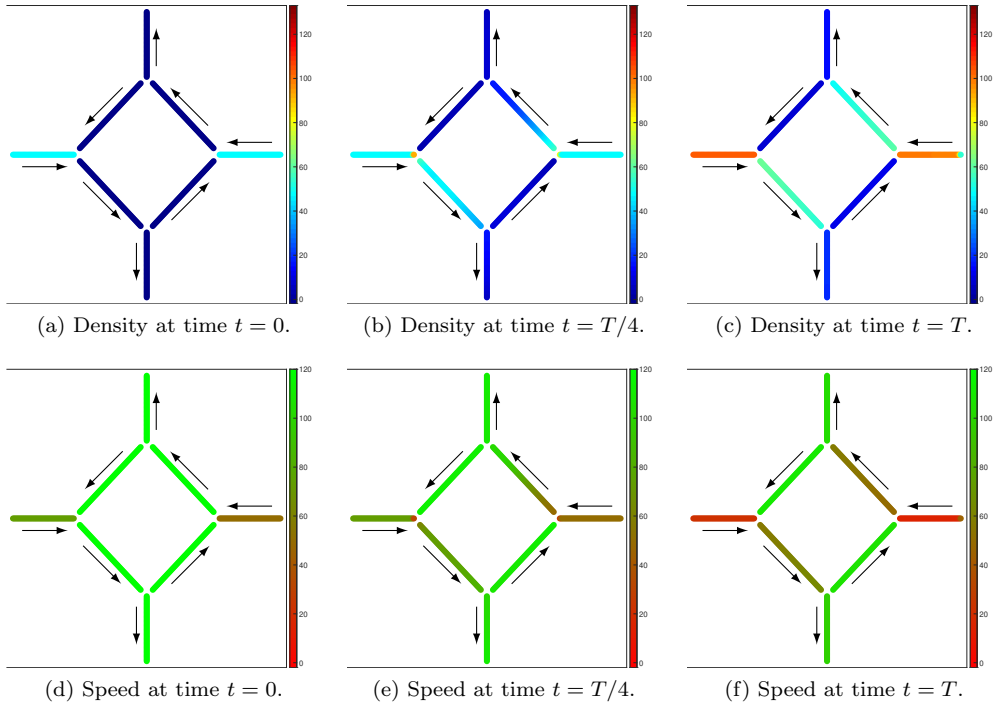


Figure 20. Test 1 roundabout: plot of density (top) and speed (bottom) of vehicles at different times with colors scaling with respect to the corresponding color-bar.

lines), since there are still no vehicles into road 8. Once vehicles of road 8 reach the right boundary, they have the priority with respect to road 1, for our choice of β , therefore we see the formation of a queue at the end of road 1. The dynamic of the density at junction J_3 represented in Figure 21(c) is quite similar, but it is slowed down by the lower value of w along the roads, see Figures 21(g) and 21(e). Such analysis is applied also to junctions J_2 and J_3 , since vehicles reach the right boundary of road 2 faster than road 6, as we can see from the red-circle lines of Figures 21(b) and 21(d), due to the different values of w . Note that the parameter α is such that there are more vehicles which exit the roundabout with respect to those which remain into it. Moreover, we observe that for the $1 \rightarrow 2$ junctions (J_2 and J_4) we have same boundary w for all the roads by construction of the solution,

except when the roads are empty. Finally, we note that the shape of the black-diamond line of Figure 21(g), which corresponds to road 6, is equal to the shape of the three lines of Figure 21(h), but with a delay. Indeed, road 6 has incoming property $w = w_6^{J_3}$, and it moves towards the road until it reaches the outgoing boundary and influences the junction J_4 .

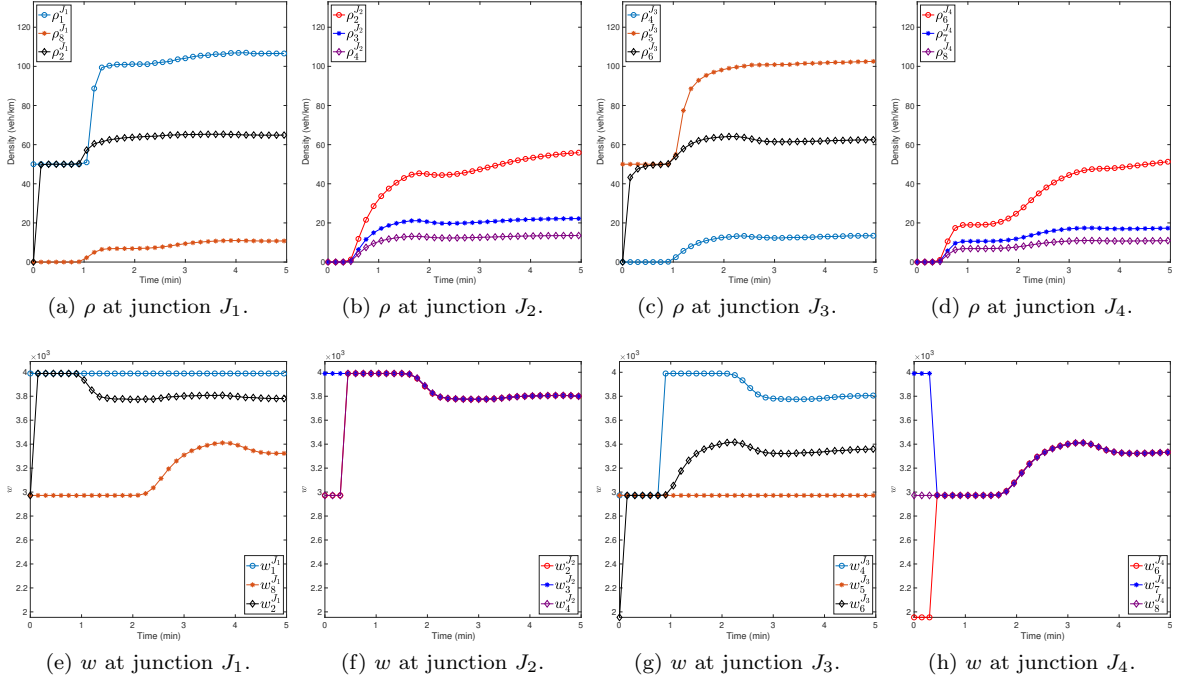


Figure 21. Test 1 roundabout: variation in time of the boundary density (top) and w (bottom) at junctions.

Now we study the decongestion of the roundabout, Figure 22, with the initial data given in the right panel of Table 4. As we can see in Figure 22(d), the different values of w define a different initial speed in road 2 and 6, even if they have same density. The emptying process is slowed down in road 6 by its lower w , which is inherited by the other roads of the roundabout during the motion. After 5 minutes of simulation the roads are almost empty.

In Figure 23 we focus again on the junctions during 10 minutes of simulation. In Figures 23(a) and 23(c) the densities corresponding to the boundary cell of roads 1 and 5 are null since no vehicles enter into the roads. The dynamic of $\rho_8^{J_1}$ and $\rho_2^{J_1}$ is quite similar, since they both decrease to 0 in time. A similar behavior also holds for $\rho_4^{J_3}$ and $\rho_6^{J_3}$. The dynamic of junction J_2 is different with respect to junction J_4 . Indeed, $\rho_2^{J_2}$ is initially constant and then it starts to decrease to 0, while $\rho_6^{J_4}$ decreases immediately to a constant value, then it increases for a while, since the road is quite full, and finally it starts to decrease to 0, as the other four roads of the two junctions. Since road 1 and 5 are always empty, in junctions J_1 and J_3 the outgoing roads inherit the property of vehicles w of the other incoming roads, and this explains why $w_2^{J_1} = w_8^{J_1}$ and $w_6^{J_3} = w_4^{J_3}$ during all the simulation. Finally we observe that the dynamic of w at junctions is cyclical, since vehicles counterclockwise move inside the roundabout until they all exit from it, except for roads 1 and 5, where anything changes during the motion.

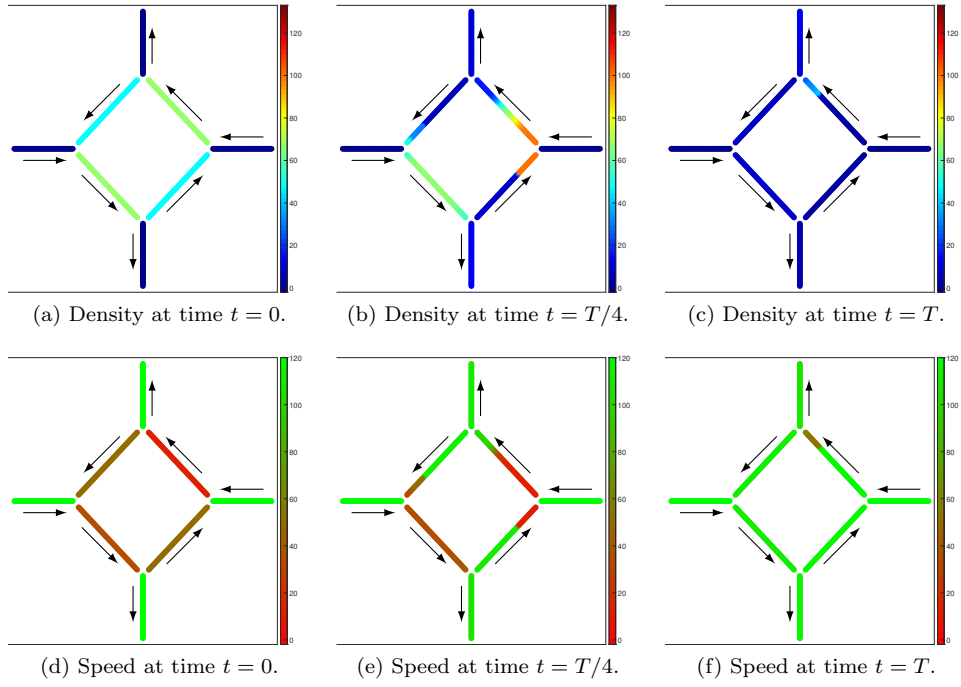


Figure 22. Test 2 roundabout: plot of density (top) and speed (bottom) of vehicles at different times with colors scaling with respect to the corresponding color-bar.

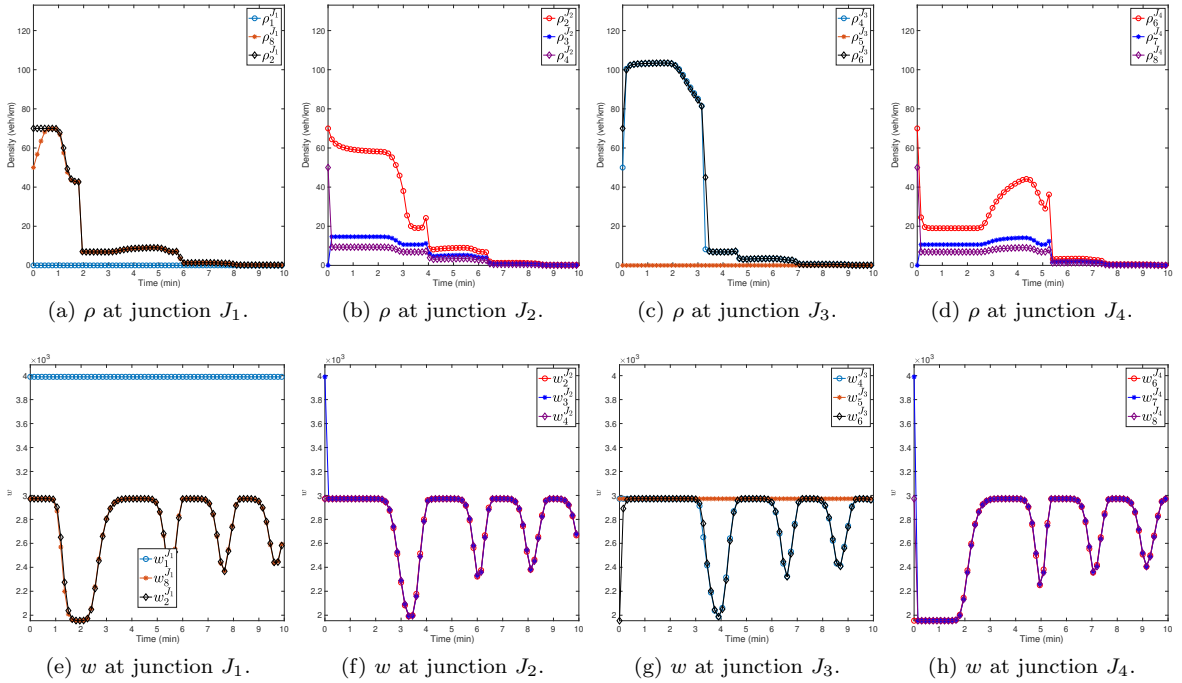


Figure 23. Test 2 roundabout: variation in time of the boundary density (top) and w (bottom) at junctions.

6 Application to NO_x emission rates

In this section we use the previous numerical test on roundabout to estimate the NO_x emission rates due to vehicular traffic. In particular, we analyze the different emission rates produced on the network when two traffic lights are placed on two of the four junctions with respect to the emissions produced on the roundabout without traffic lights.

The emission of pollutants is strictly connected to speed and acceleration of vehicles. The traffic model (2.2) gives us the speed of vehicles by means of the function $V(\rho, w)$, thus we only need to derive the acceleration. We define the function acceleration by computing the total derivative of $V(\rho, w)$, i.e.

$$a(x, t) = \frac{Dv(x, t)}{Dt} = v_t(x, t) + v(x, t)v_x(x, t),$$

where

$$v(x, t) = V(\rho(x, t), w(x, t)), \quad v_t = V_\rho \rho_t + V_w w_t, \quad v_x = V_\rho \rho_x + V_w w_x.$$

By simple computations, for the CGARZ model we have

$$a(x, t) = V_\rho (\rho_t + v \rho_x) = -V_\rho \rho v_x. \quad (6.1)$$

We now define the emission model. Following [4], we use the microscopic emission model proposed in [21]. This model estimates the microscopic emission rate E_i of vehicle i at time t using vehicle's instantaneous speed $v_i(t)$ and acceleration $a_i(t)$

$$E_i(t) = \max\{E_0, f_1 + f_2 v_i(t) + f_3 v_i(t)^2 + f_4 a_i(t) + f_5 a_i(t)^2 + f_6 v_i(t) a_i(t)\}, \quad (6.2)$$

where E_0 is a lower-bound of emission and f_1 to f_6 are emission constants, which depend on the type of pollutant and of vehicle. In particular, the coefficients associated to NO_x change with respect to the acceleration value, as shown in Table 5. In this work we take into account only the coefficients for a petrol car, for which $E_0 = 0$. We refer to [21, Table 2] for the coefficients related to the other pollutants and vehicles type.

Vehicle mode	f_1 $\left[\frac{\text{g}}{\text{s}}\right]$	f_2 $\left[\frac{\text{g}}{\text{m}}\right]$	f_3 $\left[\frac{\text{g s}}{\text{m}^2}\right]$	f_4 $\left[\frac{\text{g s}}{\text{m}}\right]$	f_5 $\left[\frac{\text{g s}^3}{\text{m}^2}\right]$	f_6 $\left[\frac{\text{g s}^2}{\text{m}^2}\right]$
If $a_i(t) \geq -0.5 \text{ m/s}^2$	6.19e-04	8e-05	-4.03e-06	-4.13e-04	3.80e-04	1.77e-04
If $a_i(t) < -0.5 \text{ m/s}^2$	2.17e-04	0	0	0	0	0

Table 5. NO_x parameters in emission rate formula (6.2) for a petrol car, [21, Table 2].

In order to work with the macroscopic variables provided by the numerical implementation of the CGARZ model, we define the emission rate of the cell x_j at time t^n as

$$E_{r,j}^n = \rho_{r,j}^n \Delta x \max\{E_0, f_1 + f_2 V_{r,j}^n + f_3 (V_{r,j}^n)^2 + f_4 a_{r,j}^n + f_5 (a_{r,j}^n)^2 + f_6 V_{r,j}^n a_{r,j}^n\}, \quad (6.3)$$

where $V_{r,j}^n$ and $a_{r,j}^n$ are the velocity and acceleration of the cell, respectively, for each road r .

6.1 A numerical test to estimate NO_x emissions

In this section we show a numerical test on a roundabout with and without traffic lights, in order to compare the resulting NO_x emission rates. We refer to Section 5.4 for the details of the traffic model on a roundabout. The procedure used is the following for each time t^n , cell x_j and road r :

1. we simulate the traffic dynamic, estimating $\rho_{r,j}^n$, $w_{r,j}^n$ and the speed $V_{r,j}^n$;
2. we compute the acceleration $a_{r,j}^n$ by means of (6.1);

3. we estimate the emission rates $E_{r,j}^n$ by means of (6.3).

The traffic simulation on the roundabout is computed with the initial data shown in Table 6 for a time of 120 min. We fix the length of each road of the roundabout equal to 3 km. We assume that vehicles enter into road 1 and 5 with density equal to 100 veh/km and 90 veh/km respectively, and that vehicles are free to leave roads 3 and 7. The parameter α of the $1 \rightarrow 2$ junctions is $\alpha = 0.4$ and the parameter β of the $2 \rightarrow 1$ junctions is $\beta = 2/3$ for junction J_1 and $\beta = 1/3$ for junction J_3 .

Road r	$\rho_{r,\cdot}^0$ (veh/km)	$w_{r,\cdot}^0$
1	100	w_R
2	0	$(w_R + w_L)/2$
3	0	w_L
4	0	$(w_R + w_L)/2$
5	90	$(w_R + w_L)/2$
6	0	w_L
7	0	w_L
8	0	$(w_R + w_L)/2$

Table 6. Initial data for the test on a roundabout to estimate the NO_x emission rates.

In order to analyze the effect of traffic lights on the roundabout, we assume to have a traffic light on junction J_1 and one on junction J_3 , with both the red and the green phase 1.5 min long. The two traffic lights are opposite, i.e. when the first one is red, the other one is green and vice versa. In this way, every 90s only vehicles from road 1 or road 8 can enter into road 2 and only vehicles from road 5 or road 4 can enter into road 6. In Figure 24 we compare the NO_x emission rates on the eight roads of the roundabout with and without traffic lights. The differences between the two scenarios are mainly related to roads involved in junctions J_1 and J_3 . The NO_x emission rates of Figures 24(a) and 24(d) both refer to the initial congestion of the roundabout. The presence of traffic lights slows down the congestion of the roundabout and thus the emissions mainly concern roads 1, 2, 5 and 6. The configuration of NO_x emissions shown in Figures 24(e) and 24(b) is quite different. Indeed, in the case without traffic lights, the NO_x emissions are going to an equilibrium, while the presence of traffic lights causes an higher production of emissions in roads 1 and 4, due to the green traffic lights which allows vehicles to leave the roads and accelerate. Finally, in Figures 24(c) and 24(f) we show the NO_x emission rates at $t = T$ and we observe that the case without traffic has reached an equilibrium while the NO_x production is significantly higher in presence of traffic lights.

In Figure 25 we compare the total emission rates along the roundabout during the 120 min of simulation. For each road r we define

$$E_r^{\text{tot}} = \sum_{j,n} E_{j,r}^n, \quad (6.4)$$

and then we sum the emissions of the eight roads, to obtain the total emission. We observe that the total amount of NO_x emissions reaches a constant value without traffic lights and a periodical behavior in presence of traffic lights. In this case, we obtain a percentage increase of 28% on the total emissions in presence of traffic lights.

7 Conclusions

In this work we have extended the Generic Second Order Models to a road network with a single merge or diverge junction, assuming the maximization of the flow and a priority rule for the incoming

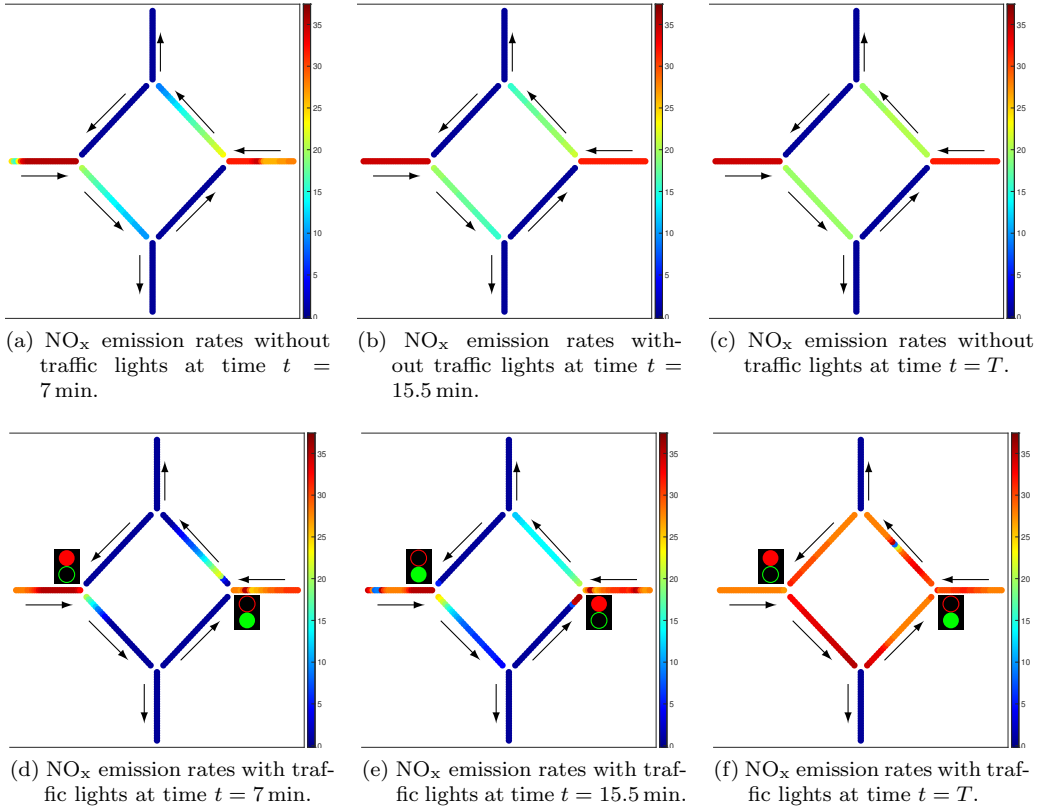


Figure 24. NO_x emission rates (g/km) on a roundabout without traffic lights (top) and with traffic lights in J_1 and J_3 (bottom).

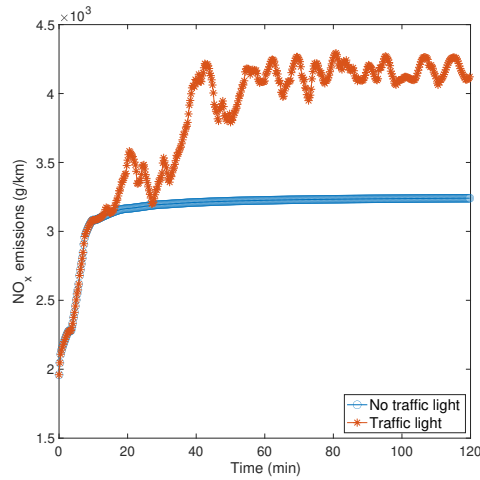


Figure 25. Total NO_x emission rates (g/km) along the whole roundabout.

roads at the merge junction. The numerical tests have shown the influence of the variable w on traffic dynamic, underlining the differences with respect to the LWR model on networks. Finally, we have estimated the NO_x emission rates produced on a roundabout, showing the increase of the emissions

in presence of traffic lights. The proposed procedure can be applied to any other pollutant associated to vehicle traffic.

References

- [1] C. APPERT-ROLLAND, F. CHEVOIR, P. GONDRET, S. LASSARRE, J.-P. LEBACQUE, AND M. SCHRECKENBERG, eds., *Traffic and granular flow '07*, Springer-Verlag, Berlin, 2009.
- [2] R. ATKINSON AND W. P. CARTER, *Kinetics and mechanisms of the gas-phase reactions of ozone with organic compounds under atmospheric conditions*, Chem. Rev., 84 (1984), pp. 437–470.
- [3] A. AW AND M. RASCLE, *Resurrection of “Second Order” Models of Traffic Flow*, SIAM J. Appl. Math., 60 (2000), pp. 916–944.
- [4] C. BALZOTTI, M. BRIANI, B. DE FILIPPO, AND B. PICCOLI, *Evaluation of NO_x emissions and ozone production due to vehicular traffic via second-order models*, arXiv preprint arXiv:1912.05956, (2019).
- [5] S. BLANDIN, D. WORK, P. GOATIN, B. PICCOLI, AND A. BAYEN, *A General Phase Transition Model for Vehicular Traffic*, SIAM J. Appl. Math., 71 (2011), pp. 107–127.
- [6] R. M. COLOMBO, *Hyperbolic Phase Transitions in Traffic Flow*, SIAM J. Appl. Math., 63 (2003), pp. 708–721.
- [7] C. F. DAGANZO, *Requiem for second-order fluid approximations of traffic flow*, Transp. Res. B, 29 (1995), pp. 277–286.
- [8] M. L. DELLE MONACHE, P. GOATIN, AND B. PICCOLI, *Priority-based Riemann solver for traffic flow on networks*, Commun. Math. Sci., 16 (2018), pp. 185–211.
- [9] S. FAN, M. HERTY, AND B. SEIBOLD, *Comparative model accuracy of a data-fitted generalized Aw-Rasclé-Zhang model*, Netw. Heterog. Media, 9 (2014), pp. 239–268.
- [10] S. FAN AND B. SEIBOLD, *Data-fitted first-order traffic models and their second-order generalizations: Comparison by trajectory and sensor data*, Transp. Res. Rec., 2391 (2013), pp. 32–43.
- [11] S. FAN, Y. SUN, B. PICCOLI, B. SEIBOLD, AND D. B. WORK, *A Collapsed Generalized Aw-Rasclé-Zhang Model and its Model Accuracy*, arXiv preprint arXiv:1702.03624, (2017).
- [12] M. GARAVELLO, K. HAN, AND B. PICCOLI, *Models for Vehicular Traffic on Networks*, American Institute of Mathematical Sciences, 2016.
- [13] M. GARAVELLO AND B. PICCOLI, *Traffic flow on a road network using the Aw-Rasclé Model*, Commun. Part. Diff. Eq., 31 (2006), pp. 243–275.
- [14] M. GARAVELLO AND B. PICCOLI, *Traffic flow on networks*, American Institute of Mathematical Sciences, 2006.
- [15] M. GARAVELLO AND B. PICCOLI, *Conservation laws on complex networks*, Ann. Inst. H. Poincaré Anal. Non Linéaire, 26 (2009), pp. 1925–1951.
- [16] M. HERTY, S. MOUTARI, AND M. RASCLE, *Optimization criteria for modelling intersections of vehicular traffic flow*, Netw. Heterog. Media, 1 (2006), pp. 275–294.
- [17] M. HERTY AND M. RASCLE, *Coupling conditions for a class of second-order models for traffic flow*, SIAM J. Math. Anal., 38 (2006), pp. 595–616.

- [18] H. HOLDEN AND N. H. RISEBRO, *A mathematical model of traffic flow on a network of unidirectional roads*, SIAM J. Math. Anal., 26 (1995), pp. 999–1017.
- [19] J.-P. LEBACQUE, S. MAMMAR, AND H. HAJ-SALEM, *Generic second order traffic flow modelling*, in Transportation and Traffic Theory, Elsevier, 2007, pp. 755–776.
- [20] M. J. LIDTHILL AND G. B. WHITHAM, *On kinematic waves II. A theory of traffic flow on long crowded roads*, Proc. Roy. Soc. A, 229 (1955), pp. 317–345.
- [21] L. I. PANIS, S. BROEKX, AND R. LIU, *Modelling instantaneous traffic emission and the influence of traffic speed limits*, Sci. Total Environ., 371 (2006), pp. 270–285.
- [22] H. J. PAYNE, *Models of freeway traffic and control*, Proc. Simulation Council, 1 (1971), pp. 51–61.
- [23] B. PICCOLI, K. HAN, T. L. FRIESZ, T. YAO, AND J. TANG, *Second-order models and traffic data from mobile sensors*, Transport. Res. C-Emer., 52 (2015), pp. 32 – 56.
- [24] P. I. RICHARDS, *Shock Waves on the Highway*, Operations Research, 4 (1956), pp. 42–51.
- [25] G. B. WHITHAM, *Linear and nonlinear waves*, John Wiley and Sons, New York, 1974.
- [26] H. M. ZHANG, *A non-equilibrium traffic model devoid of gas-like behavior*, Transp. Res. B, 36 (2002), pp. 275–290.
- [27] K. ZHANG AND S. BATTERMAN, *Air pollution and health risks due to vehicle traffic*, Sci. Total Environ., 450-451 (2013), pp. 307 – 316.